SUPPLEMENTARY INFORMATION

A cobalt phosphide catalyst for the hydrogenation of nitriles

Takato Mitsudome,* Min Sheng, Ayako Nakata, Jun Yamasaki, Tomoo Mizugaki, Koichiro Jitsukawa

*Correspondence to: mitsudom@cheng.es.osaka-u.ac.jp

Table of Contents

1. Recycling experiments

After the reaction, the crude reaction mixture was centrifuged to obtain the reaction solution and the yield was determined by GC analysis. Nano-Co_2P/HT was redispersed in 2-propanol (3 mL) and placed in a 50-mL stainless-steel autoclave again with addition of nitrile (0.5 mmol), and NH_3 aq. (25%, 1.2 mL) for reuse experiments. The TEM images of the used nano-Co_2P/HT catalyst (Fig. S1) showed that the average diameter and size distribution of the nano-Co_2P were similar to those of nano-Co_2P/HT before use and no aggregation of nano-Co_2P occurred, proving high durability of nano-Co_2P/HT against aggregation.

2. Characterization

Table S1 The elemental analysis of fresh and used nano-Co_2P/HT.

	wt%		
	Mg	Al	Co
nano-Co_2P/HT _fresh	19.2	7.17	1.23
nano-Co_2P/HT_after_reaction	22.3	8.04	1.16

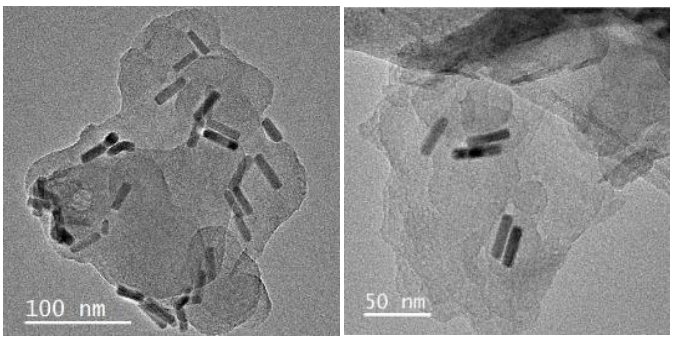

Fig. S1 TEM images of nano-Co_2P/HT fresh (left) and after reaction (right).

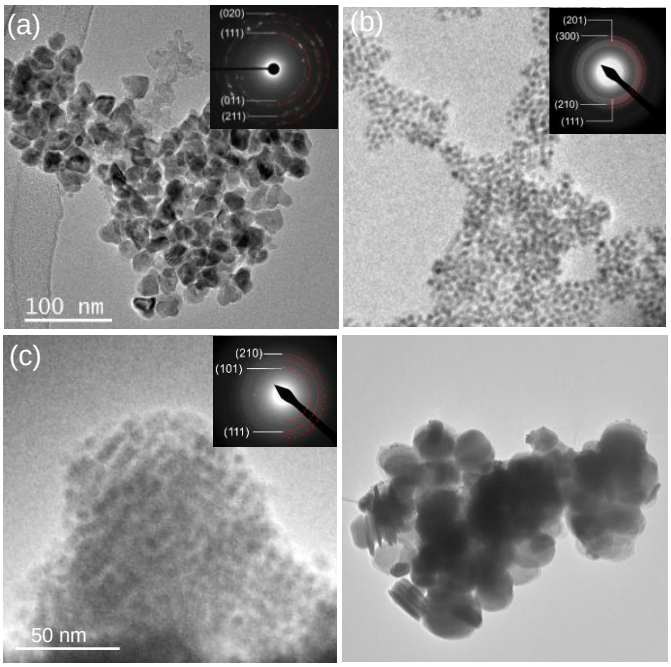

Fig. S2 TEM images of (a) nano-CoP, (b) nano-Ni_2P, (c) nano-Fe_2P and (d) nano-Cu_3P with SAED pattern (inset) (S1-4).

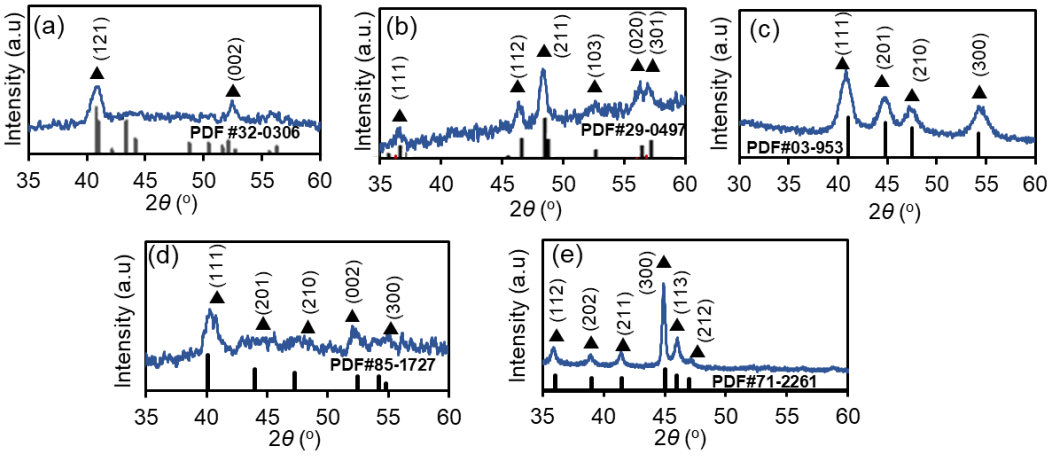

Fig. S3 XRD patterns of (a) nano-Co_2P, (b) nano-CoP, (c) nano-Ni_2P, (d) nano-Fe_2P and (e) nano-Cu_3P with PDF reference patterns (S5-8).

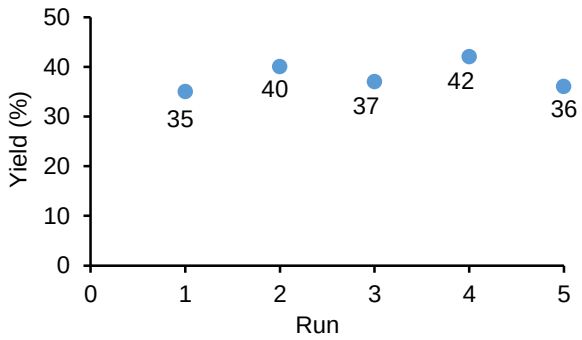

Fig. S4 Reuse experiments of nano-Co_2P/HT for valeronitrile hydrogenation at 50% conversion. Reaction conditions: nano-Co_2P/HT (0.1 g), valeronitrile (0.5 mmol), 2-propanol (3 mL), NH_3 aq. (0.8 mL), 130 °C, 40 bar H_2, 20 min.

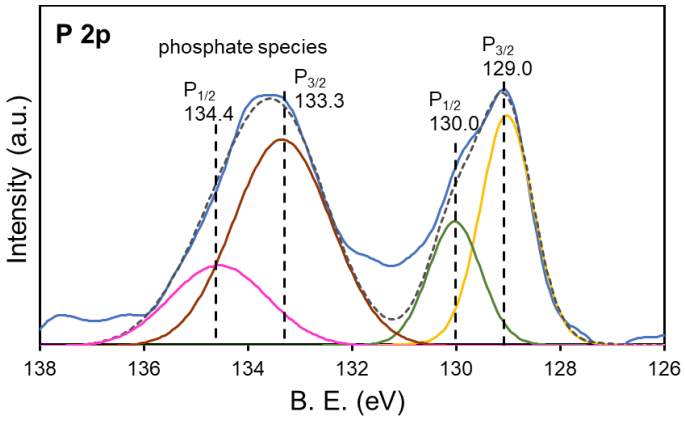

Fig. S5 XPS result of P 2p region of nano-Co_2P (S9-10).

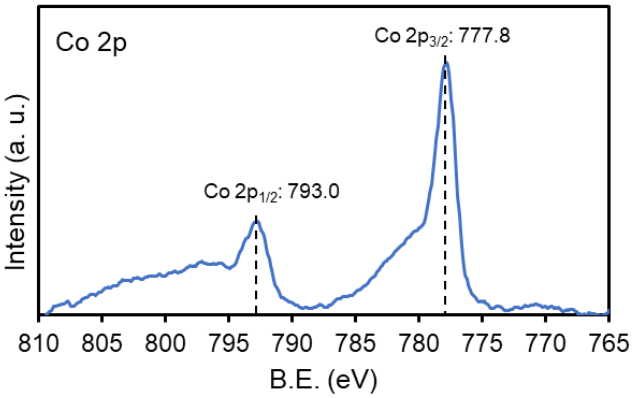

Fig. S6 XPS result of Co 2p region of recovered nano-Co_2P.

3. Comparison of activity between nano-Co_2P and reported nonprecious metal catalysts

Table S2 Comparison of activity between nano-Co_2P and reported nonprecious metal catalysts for nitrile hydrogenation.

Entry	Catalyst	Active metal	Reaction condition	TON	reference
1	nano-Co_2P/HT	Co	0.017 mol% catalyst, NH_3 aq., 50 bar, 150 °C, 40 h.	58800 (5000 based on total cobalt atoms)	This work
2	{Fe(H)(HBH_3)(CO)[(CH_3)N((CH_2CH_2)P($CH(CH_3)_2$)$_2$)$_2$]}	Fe	0.5−1 mol% catalyst, 30 bar H_2, 70−130 °C, 3−6 h.	174	*Nat. Commun.* 54111 (2014)
3	Fe(PNP)Br_2 Complex	Fe	1−5 mol% catalyst, 1−5 mol% $NaHBEt_3$, 3−15 mol% KHMDS, 60 bar H_2, 140 °C, 19−48 h.	100	*Chem. Commun.* **52,** 1812–1815 (2016)
4	Fe(PNP^{Cy})	Fe	0.5−1 mol% catalyst, 30 bar H_2, 40−70 °C, 2−3 h.	190	*Catal. Sci. Technol.* **6,** 4768–4772 (2016)
5	Co PNNH Pincer Complex	Co	2 mol% catalyst, 2 mol% $NaEt_3BH$, 4.4 mol% KO*t*Bu, 30 bar H_2, 135°C, 36−60 h.	100	*J. Am. Chem. Soc.***137,** 8888–8891 (2015)
6	(^{Mes}CCC)-$CoCl_2$py Catalyst Precursor	Co	4 mol % catalyst, 8 mol % $NaHBEt_3$, 12 mol % KO*t*Bu, 4 bar, 115°C, 8 h.	25	*J. Am. Chem. Soc.* **139,** 13554–13561 (2017)
7	$Co(acac)_3$ + Tetradentate phosphine	Co	4 mol% $Co(acac)_3$, 4.4 mol% tetradentate phosphine, 10 mol% KO*t*Bu, 30 bar H_2, 80−120°C, 18 h.	25	*ChemSusChem* **10,** 842–846 (2017)
8	$CoBr_2$ with	Co	2 mol% $CoBr_2$, 6 mol%	48	*ACS Catal.* **8,**

	$NaHBEt_3$ + HN-($CH_2CH_2P^iPr_2$)$_2$ ($^{iPr}PN^HP$)		$NaHBEt_3$, 20 or 40 bar H_2, 110 or 130 °C, 4−24 h.		9125–9130 (2018)
9	Zr_{12}-TPDC-Co	Co	0.5 mol% catalyst, 40 bar H_2, 110 °C, 42 h.	200	*J. Am. Chem. Soc.* **139,** 7004–7011 (2017)
10	$Co(OAc)_2$/Phen@ α-Al_2O_3	Co	4−6 mol% catalyst, 5−40 bar H_2, 85−130 ^oC, 2−24 h.	25	*J. Am. Chem. Soc.* **138,** 8781−8788 (2016)
11	Cobalt-terephthalic acid MOF@C-800	Co	3.8 mol% catalyst, 25 bar H_2, 5 bar NH_3, 120 ^oC, 16 h.	25	*Chem. Sci.* **9,** 8553–8560 (2018)
12	Co_3O_4/ NGr@CeO_2	Co	1.6−5 mol% catalyst, aqueous NH_3, 30−50 bar H_2, 120 °C, 8−15 h.	62	*Catal.Sci.Technol.***8,** 499–507 (2018)
13	Manganese Pincer Complexes	Mn	3 mol% catalyst, *t*-BuONa, 50 bar H_2, 120 °C, 24 h.	33	*J. Am. Chem. Soc.* **138,** 8809–8814 (2016)
14	*Fac*-[$(CO)_3$Mn(dippe)(OTf)]	Mn	3 mol% catalyst, 10 mol% KO*t*Bu, 7-35 bar H_2, 90 °C, 15−30 min.	31	*ACS Catal.* **9,** 392–401 (2019)
15	Bisphosphine Mn(I) Complex	Mn	2 mol % catalyst, 20 mol % *t*-BuOK, 100 °C, 50 bar H_2, 18 h.	48	*Org. Lett.* **20,** 7212–7215 (2018)
16	MC/Ni Catalyst	Ni	13 mol % MC/Ni catalyst, NH_3 aq. (36 wt. %), 2.5 bar H_2, 80°C, 6−18 h.	8	*ChemSusChem* **12,** 1–11 (2019)
17	Ni nanoparticles embedded in imidazolium based ionic liquids	Ni	0.7 mol% based on the Ni precursor, 20−30 bar H_2, 90°C, 22 h.	1021 (143 based on total nickel atoms)	*New J. Chem.*, **41**, 9594–9597 (2017)
18	Ni/Al_2O_3-600	Ni	20 mg catalyst, 2.5 bar H_2, $NH_3 \cdot H_2O$ (36.5 wt%), 60 °C, 6 h.	8	*New J. Chem.*, **44**, 549-555 (2020)
19	Ni-phen@SiO_2	Ni	45 mg catalyst (4.5 mol % Ni), 50 bar H_2, 100°C, 7 M NH_3/MeOH, 20 h.	22	*Sci. Adv.* **4**, eaat0761, (2018)
20	Cu/SiO_2 with H_2 pretreatment	Cu	6 mol % catalyst, 13−40 bar H_2, 110−130°C, 9−20 h.	12	*Applied Catalysis A: General* **494**, 41–47 (2015)

4. DFT calculation

Density functional theory (DFT) calculations were performed using the CONQUEST

program (S11). The Perdew, Burke and Ernzerhof (PBE) exchange-correlation functional (S12) was used with a norm-conserving pseudopotential and real-space pseudo atomic orbitals (PAOs) (S13). We used the double-zeta plus polarization (DZP) type PAOs. The ranges of two *s*, two *d* and a *p* PAOs for Co were {(7.8, 6.1), (4.5, 2.1) and (7.8)} bohr and those of two *s*, two *p* and a *d* PAOs for P were {(5.2, 4.0), (6.5, 4.6) and (6.5)} bohr.

Bulk Co, Co_2P and Co_2P surface

8×8×8 Monkhorst–Pack grid (S14) was used for the bulk Co and Co_2P in the present calculations. The unit cells of the bulk Co and Co_2P were rectangular in the present calculations. The c/a ratios of the unit cells were fixed to the experimental ratios, 1.623 (S15) and 0.602 (S16) for bulk Co and Co_2P, and the b/a ratio was $\sqrt{3}$. As shown in Fig. 6c, the unit cell of Co_2P consists of two layers, six Co atoms in the pyramidal site (P-site) and two P atoms in the first layer and six Co atoms in the tetrahedral site (T-site) and four P atoms in the second layer. For the calculation of the Co_2P (0001) surface, we used a supercell slab consisting of eight layers (about 12 Å thickness) with a vacuum gap (about 15 Å). 8×8×1 grid was used for the surface system. All atoms were relaxed in the geometry optimizations of bulk Co (hcp), bulk Co_2P (hexagonal) and the Co_2P surface systems. The lattice constants of bulk Co_2P calculated with the PAOs were very close to those with the plane-wave functions (S17), as shown in Table S3.

Table S3 Lattice constants of hexagonal Co_2P (Å).

	Nonmagnetic		Ferromagnetic	
	a	c	a	c
PAOs	5.754	3.452	5.767	3.460
Plane waves[a]			5.723	3.406
Exptl.[b]			5.742	3.457

[a] Reference S16, [b] Reference S17

Projected density of states (PDOS) of bulk Co, Co_2P and the Co_2P surface system are shown in Fig. S7, which were calculated based on the PAOs, i.e., the projection weights were determined using the PAO-based band coefficients. Since it was found experimentally that the nano-Co_2P doesn't have magnetism, the magnetism was not considered in the present calculations. In Fig. S7, the increase of *d*-electrons around Fermi level is found both for P- and T-site Co atoms in the Co_2P surfaces. The comparison of the Co-*d* PDOS is given in Fig. 6 for T-site Co.

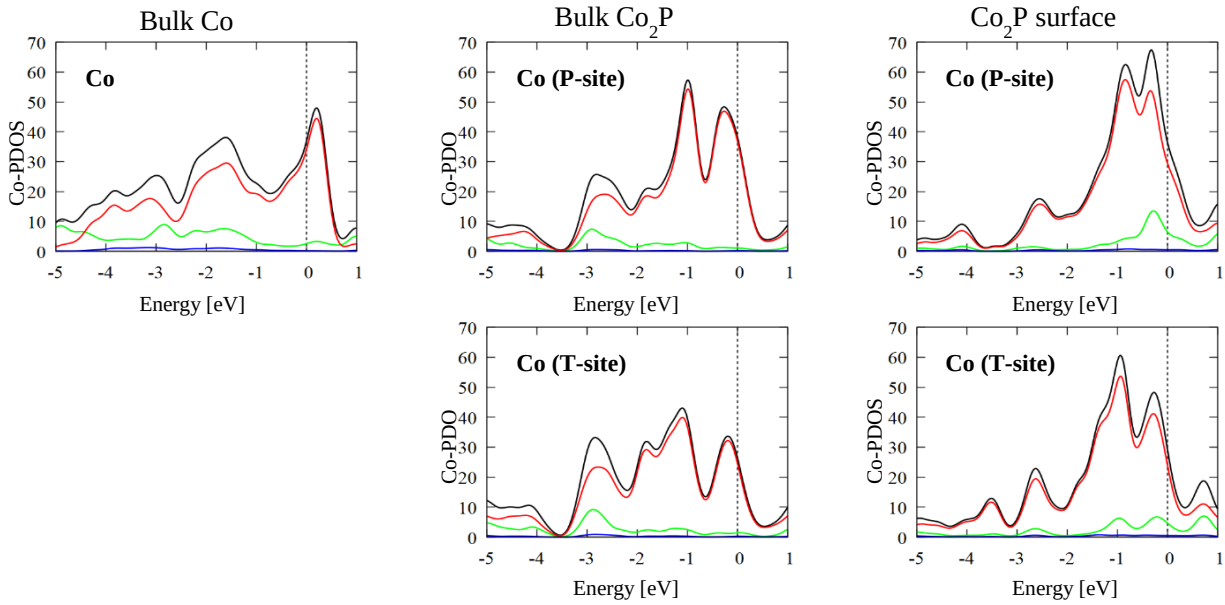

Fig. S7 PDOS of Co atoms in bulk Co, bulk Co_2P and Co_2P surface (green: *s* orbital, blue: *p* orbital, red: *d* orbital, black: total). Fermi level is set to be zero.

H_2 on Co_2P surface

The dissociation of a H_2 molecule on Co_2P surfaces was simulated. We first put a H_2 molecules on the Co_2P surface with the distance of 1.2 Å and then relaxed the geometry. Only the geometries of the H_2 molecule and the first and second layers of Co_2P were relaxed, while the Co_2P consisted of 8 layers. Several H_2 positions were investigated as shown in Fig. S8. The increases of the Co *d*-electrons around Fermi level are found both for P- and T-sites Co atoms. The comparison of the Co-*d* PDOS is given in Fig. 6 for T-site Co. The distances of the two H atoms ($r_{H–H}$) and the adsorption energies are presented in Fig. S8. The stabilization energy ΔE was calculated as

$\Delta E = E(Co_2P\text{-}H_2) – E(Co_2P) – E(H_2)$.

The dispersion energies were considered by using the DFT-D2 method (S18). The basis set superposition errors (BSSEs) were corrected by the counterpoise method (S19). The H_2 molecules are dissociated largely when adsorbing to the bridge and hollow sites in Fig. S8. When a H_2 molecule adsorbs to the on-top site, the two H atoms are bonded to the nearest Co atom, while the distance between two H atoms is longer than an isolated H_2 molecule (0.79 Å). In the optimized geometry of “bridge 2” of T-site layer, the H atoms are located at the different hollow sites.

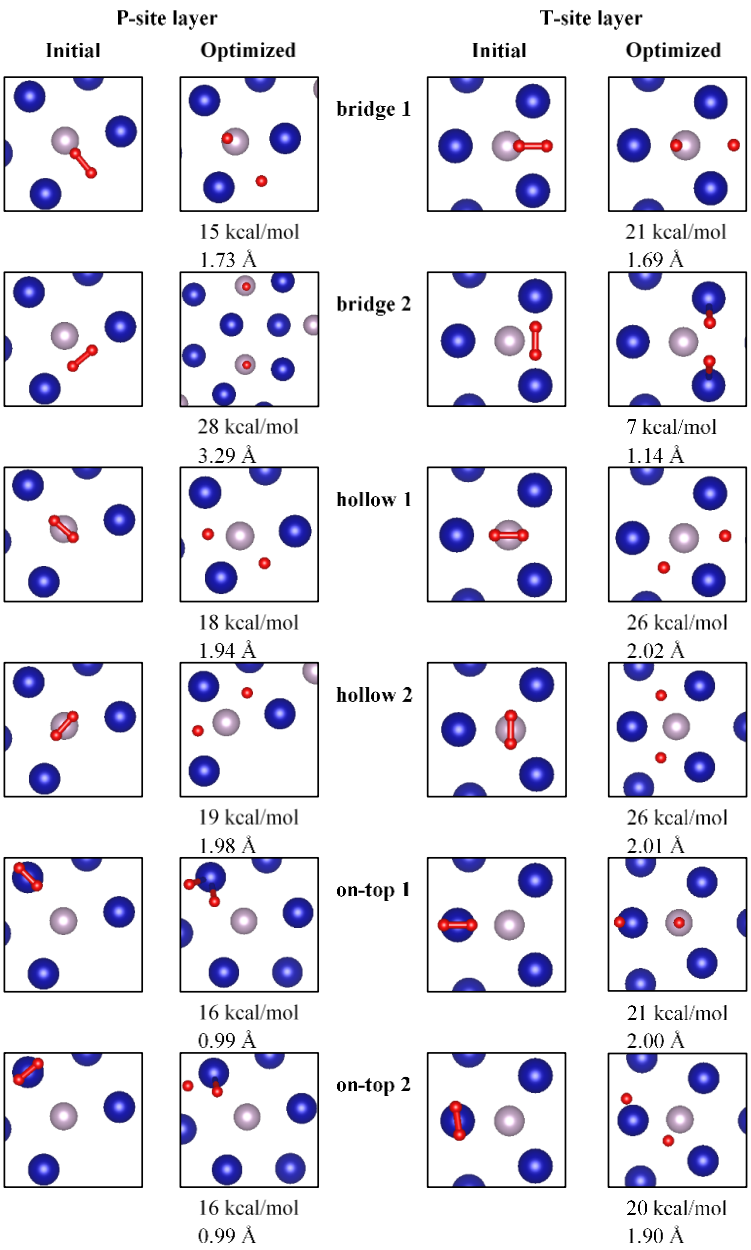

Fig. S8. Initial and optimized structures of the H_2 molecules on Co_2P (0001) surface. Co, P, and H atoms are coloured in blue, pink and red. H–H distances in the initial structures are 0.79 Å. H–H distances and the adsorption energies in the optimized structures are written in the figure.

5. Product identification

Table 1, **1b**

***n*-Pentylamine hydrochloride (*S20*)**

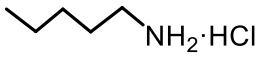

CAS registry No. [142-65-4]. ^{1}H NMR (DMSO, 400 MHz): δ = 7.95 (s, 3H), 2.73 (t, *J* = 7.3, 2H), 1.56 (m, 2H), 1.33-1.26 (m, 4H), 0.88 (t, *J* = 6.8, 3H). ^{13}C NMR (DMSO, 100 MHz): 38.7, 27.9, 26.5, 21.5, 13.6.

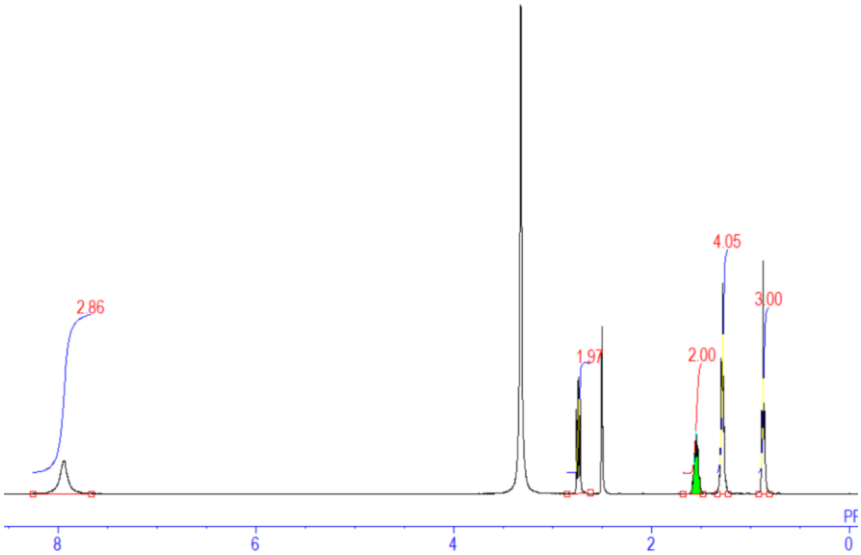

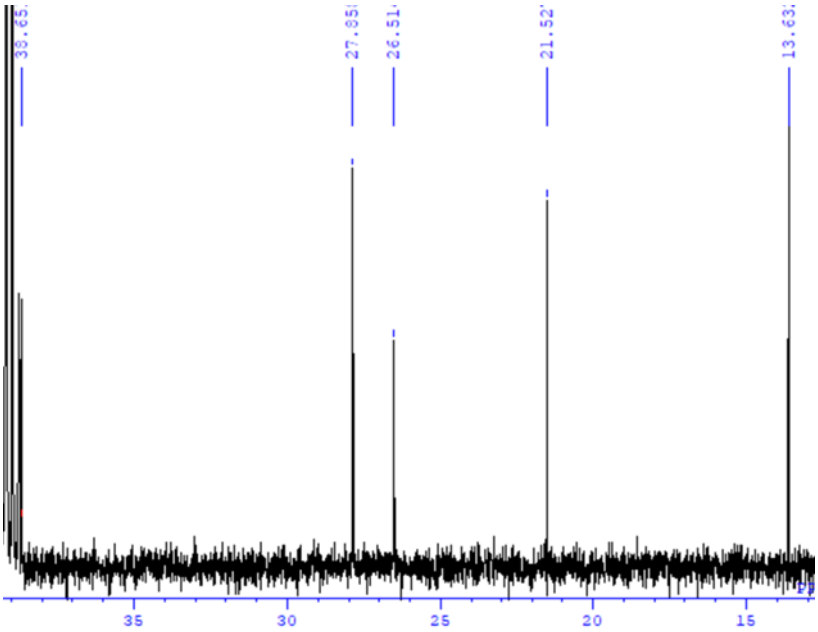

Table 1, **2b**

1-Cyclohexylmethanamine hydrochloride (*S20*)

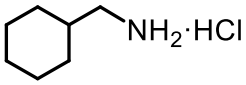

CAS registry No. [50877-01-5]. ^{1}H NMR (DMSO, 400 MHz): δ = 7.84 (s, 3H), 2.62 (d, *J* = 6.4, 2H), 1.69 (m, 4H), 1.53 (m, 2H), 1.16 (m, 3H), 0.91 (m, 2H). ^{13}C NMR (DMSO, 100 MHz): 44.3, 35.3, 29.6, 25.5, 25.0.

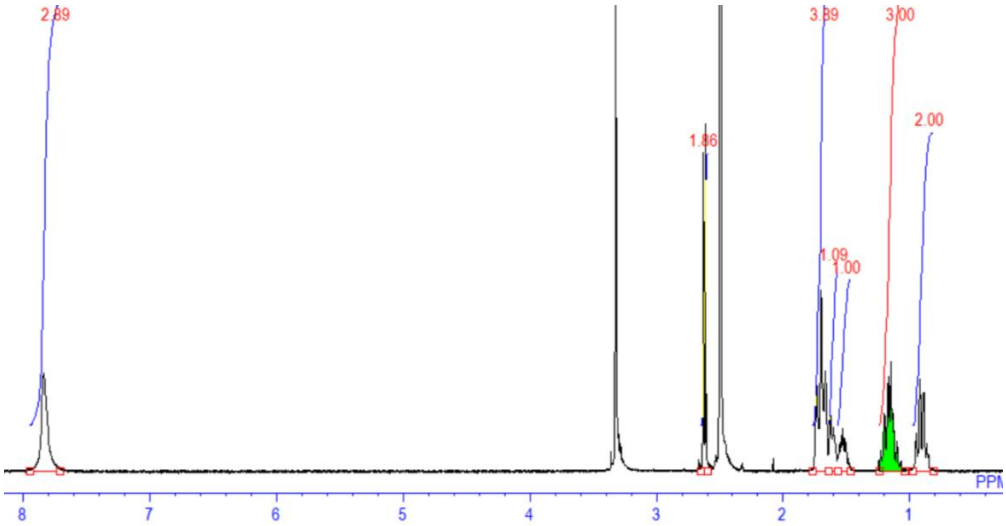

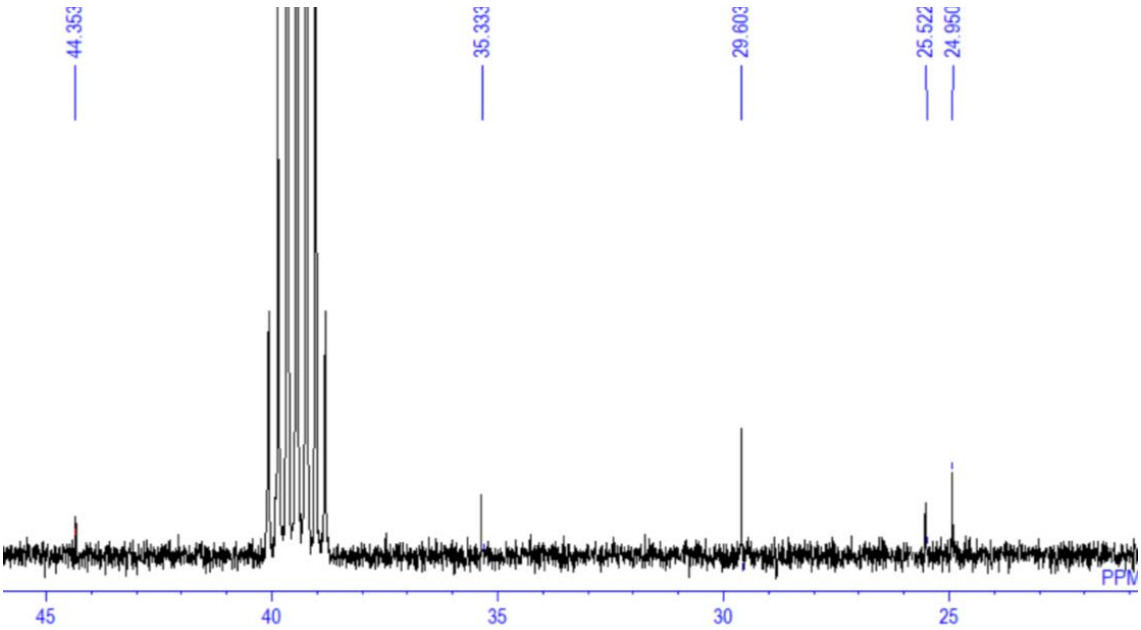

Table 1, **3b**

Decylamine hydrochloride (*S22*)

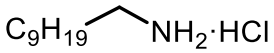

CAS registry No. [143-09-9]. ^{1}H NMR (DMSO, 400 MHz): δ = 7.75 (s, 3H), 2.75 (t, *J* = 8.5, 2H), 1.51 (m, 2H), 1.25 (m, 14H), 0.86 (t, *J* = 7.6, 3H). ^{13}C NMR (100 MHz, DMSO): 38.7, 31.2, 28.8, 28.7, 28.6, 28.4, 26.9, 25.7, 22.0, 13.9.

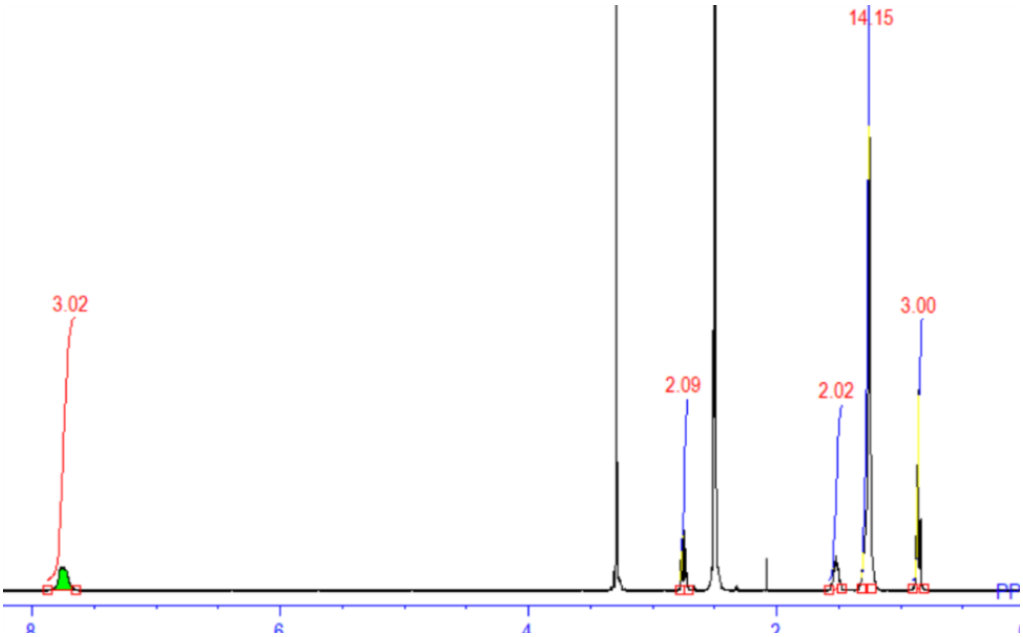

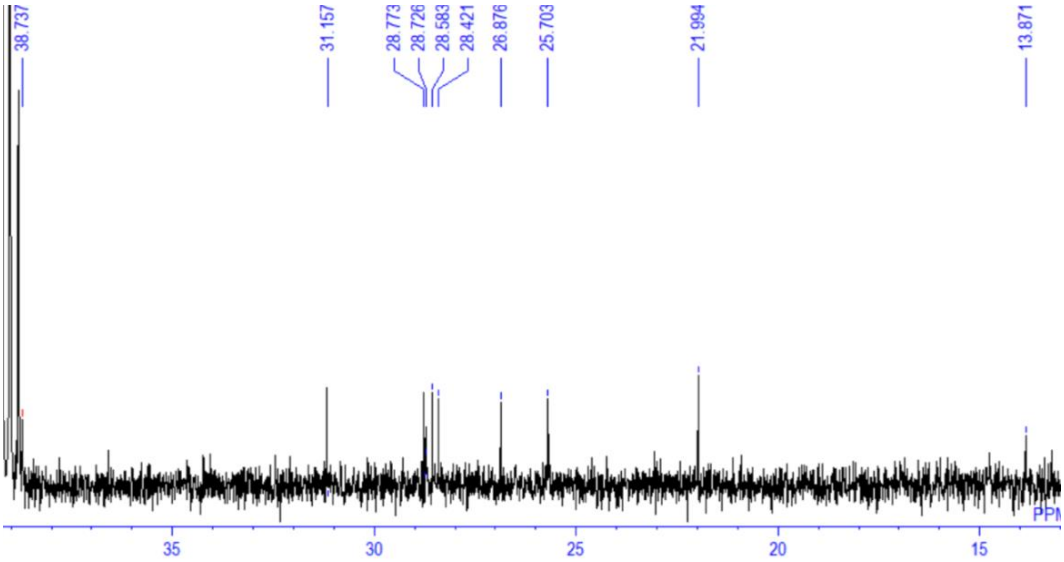

Table 1, **4b**

1-Adamantylmethylamine hydrochloride (*S21*)

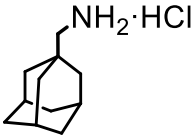

CAS registry No. [1501-98-0]. ^{1}H NMR (DMSO, 400 MHz): δ = 7.76 (s, 3H), 2.48 (s, 2H), 1.96 (s, 3H), 1.68 (d, *J* = 11.9, 3H), 1.59 (d, *J* = 11.4, 3H), 1.50 (s, 6H). ^{13}C NMR (DMSO, 100 MHz): 49.9, 38.7, 36.0, 30.5, 27.4.

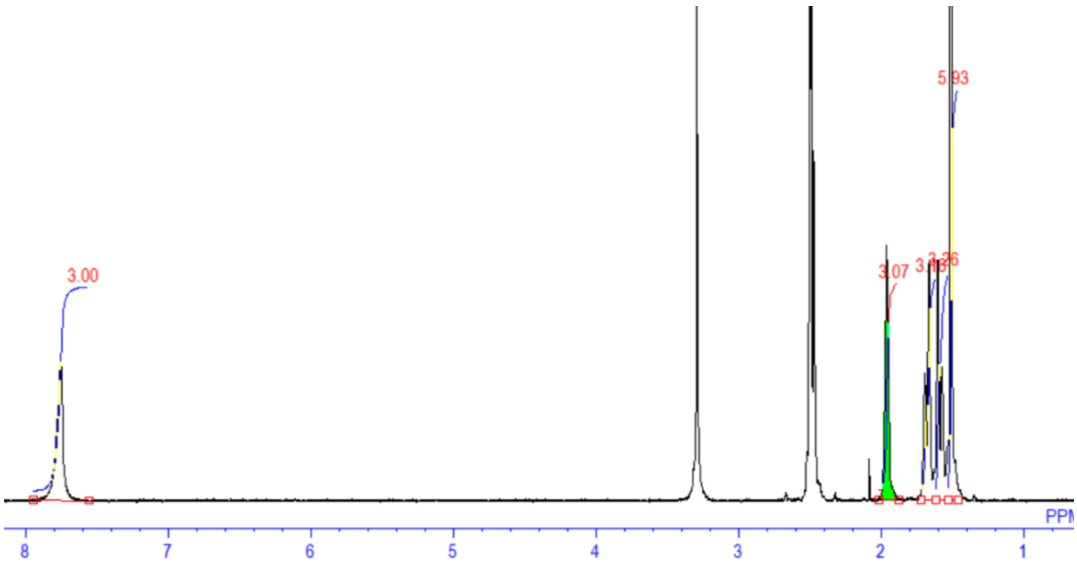

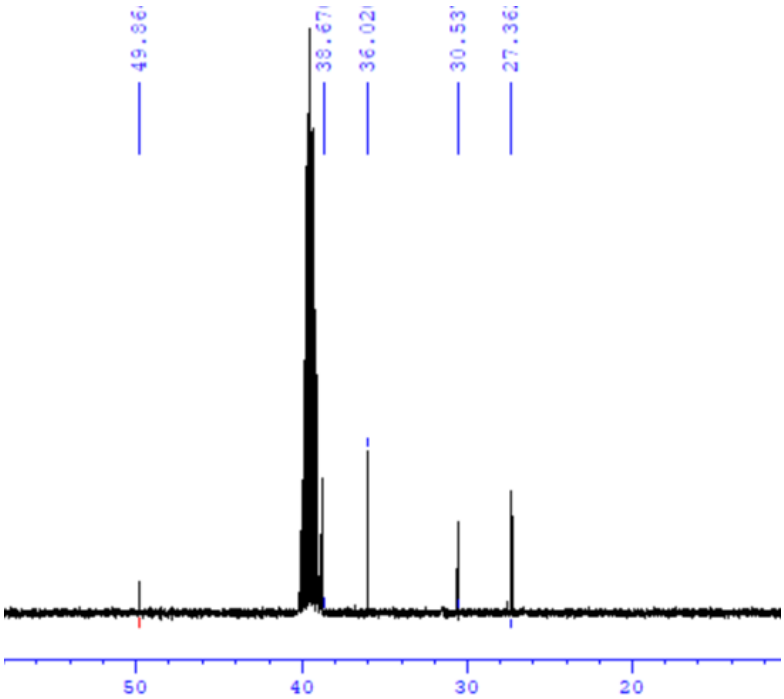

Table 1, **5b**

Benzylamine hydrochloride (*S21*)

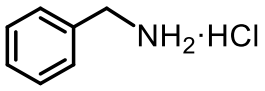

CAS registry No. [3287-99-8]. ^{1}H NMR (DMSO, 400 MHz): δ = 8.05 (s, 3H), 7.30 (m, 5H), 3.01 (s, 2H). ^{13}C NMR (DMSO, 100 MHz): 134.0, 128.9, 128.5, 128.3, 42.1.

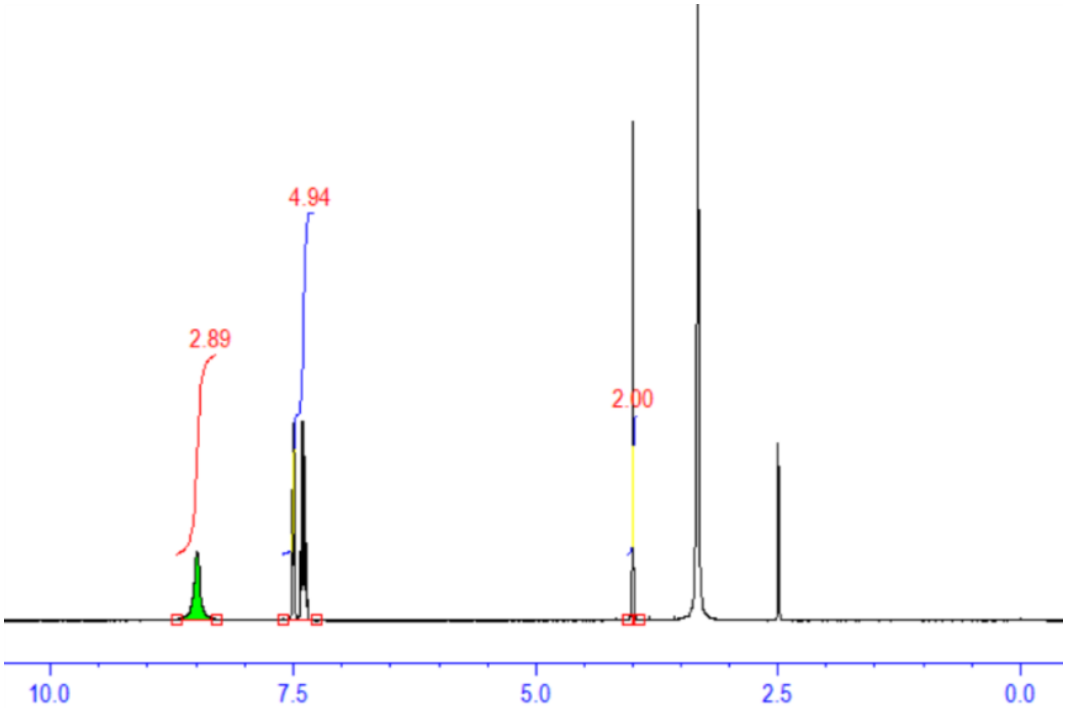

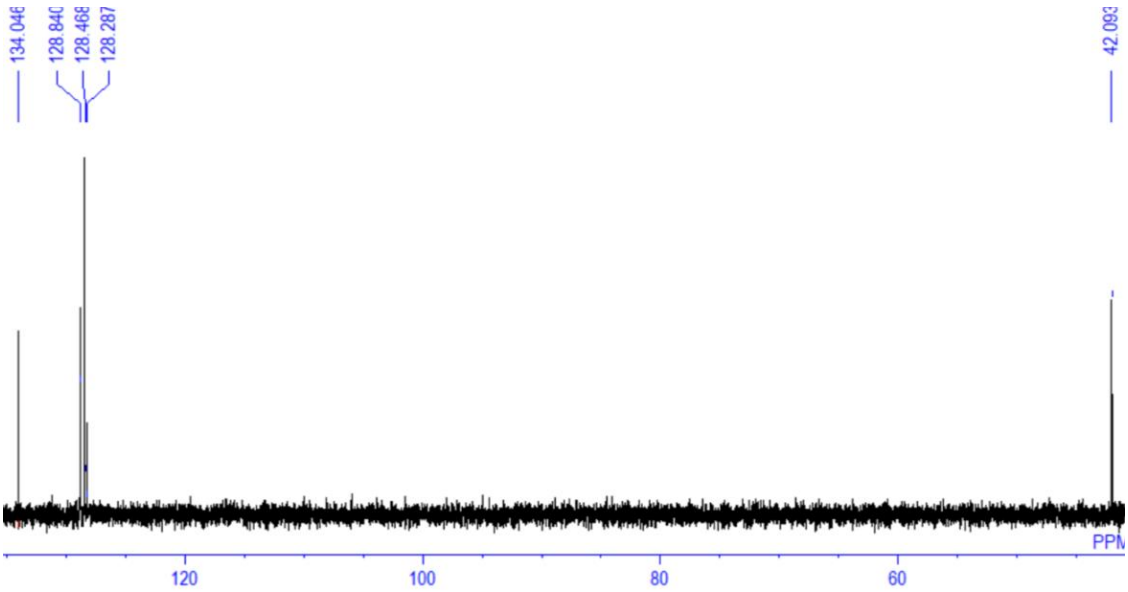

Table 1, **6b**

2-Phenylethylamine hydrochloride (*S21*)

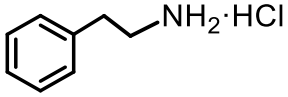

CAS registry No. [156-28-5]. ^{1}H NMR (DMSO, 400 MHz): δ = 8.07 (s, 3H), 7.36-7.23 (m, 5H), 3.10-2.82 (m, 4H). ^{13}C NMR (DMSO, 100 MHz): 137.4, 128.53, 128.52, 126.6, 39.8, 32.9.

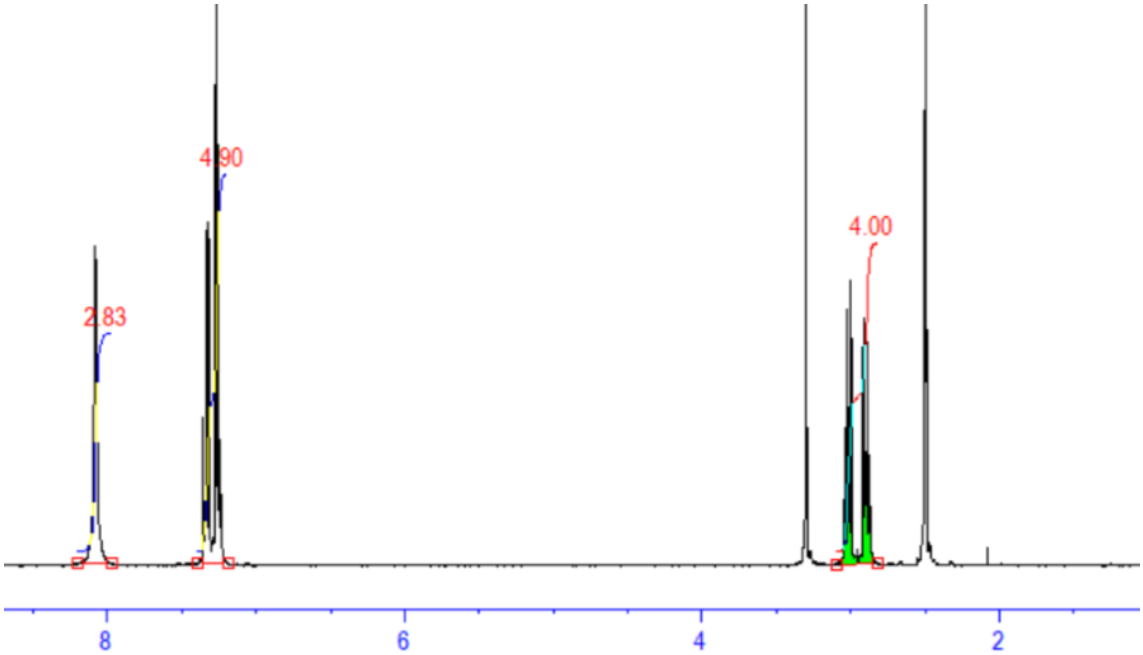

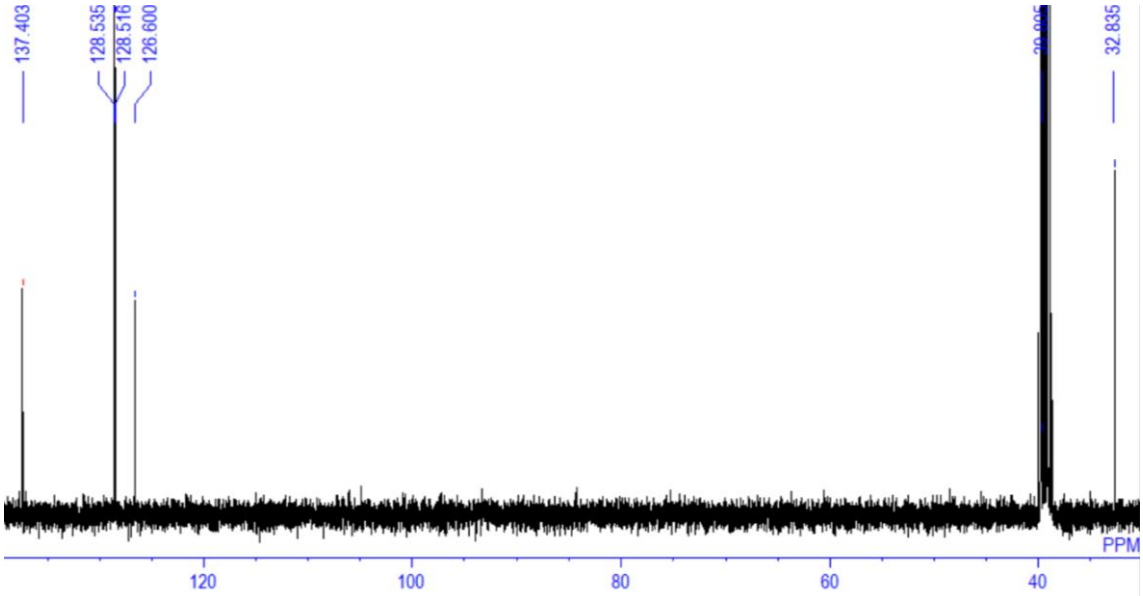

Table 1, **7b**

3-Picolylamine hydrochloride (*S23*)

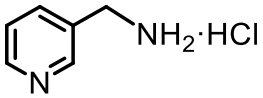

CAS registry No. [84359-15-9]. ^{1}H NMR (DMSO, 400 MHz): δ = 8.78(s, 1H), 8.72-8.43 (m, 4 H), 8.10 (d, *J* = 5.7, 1H), 7.60 (t, *J* = 8.0, 1H), 4.21 (s, 2H). ^{13}C NMR (DMSO, 100 MHz): 66.3, 38.6, 28.6, 28.4, 26.8, 25.7.

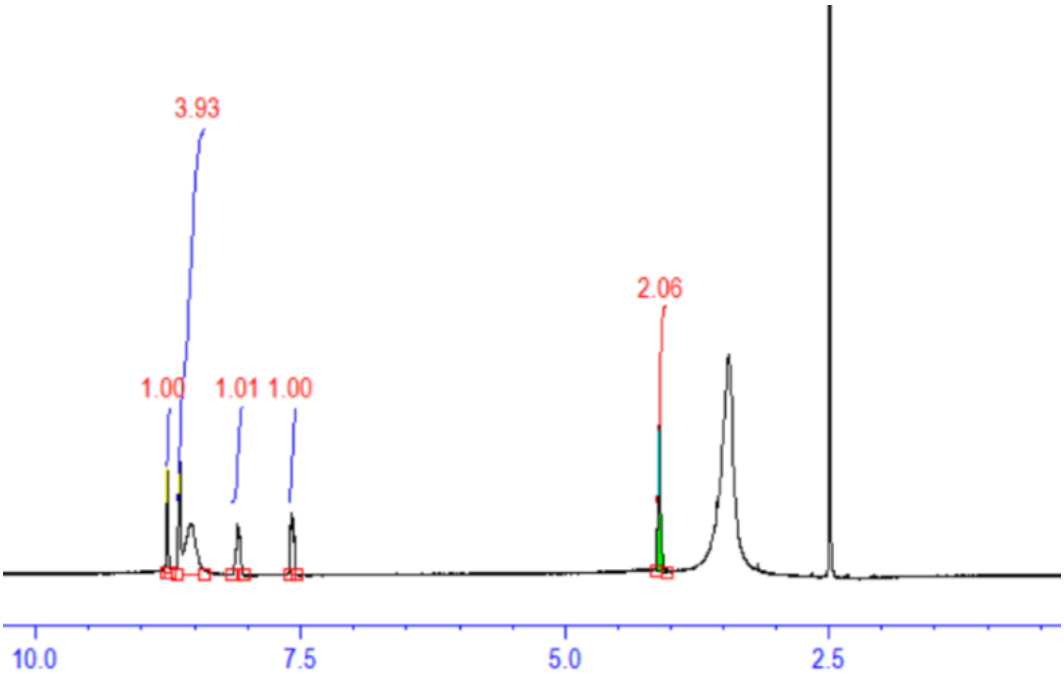

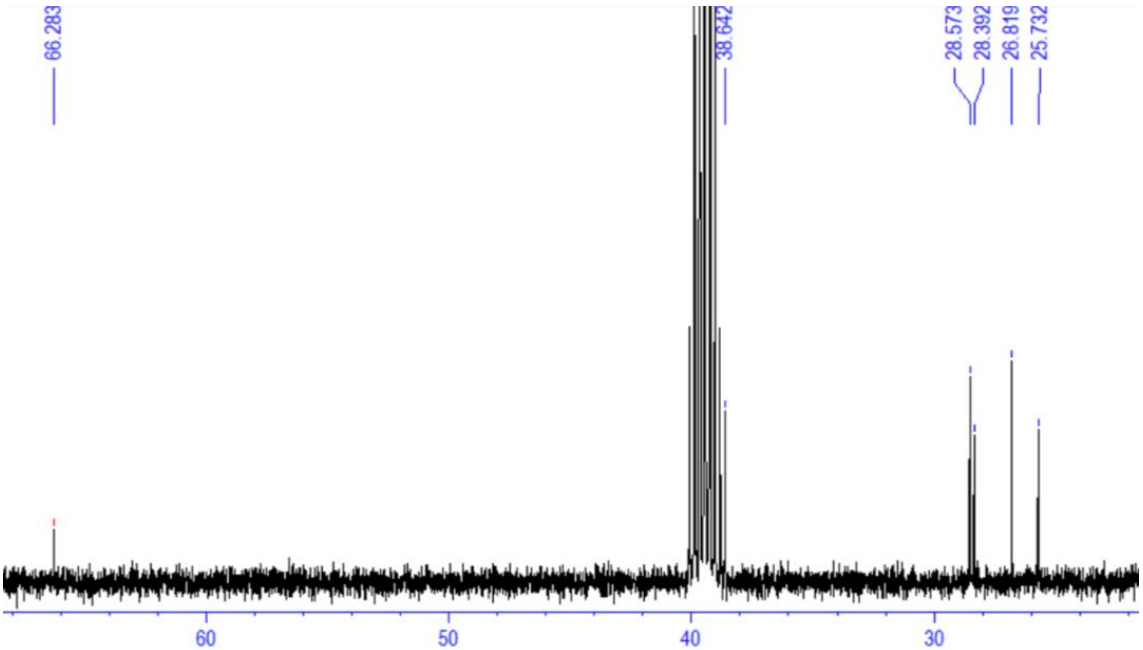

Table 1, **8b**

4-Picolylamine hydrochloride (*S24*)

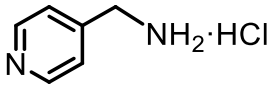

CAS registry No. [64460-41-9]. ^{1}H NMR (DMSO, 400 MHz): δ = 8.61 (s, 2H), 7.52 (d, 2H, *J* = 4.4), 4.19 (s, 2H). ^{13}C NMR (DMSO, 100 MHz): 149.6, 143.8, 123.2, 41.2.

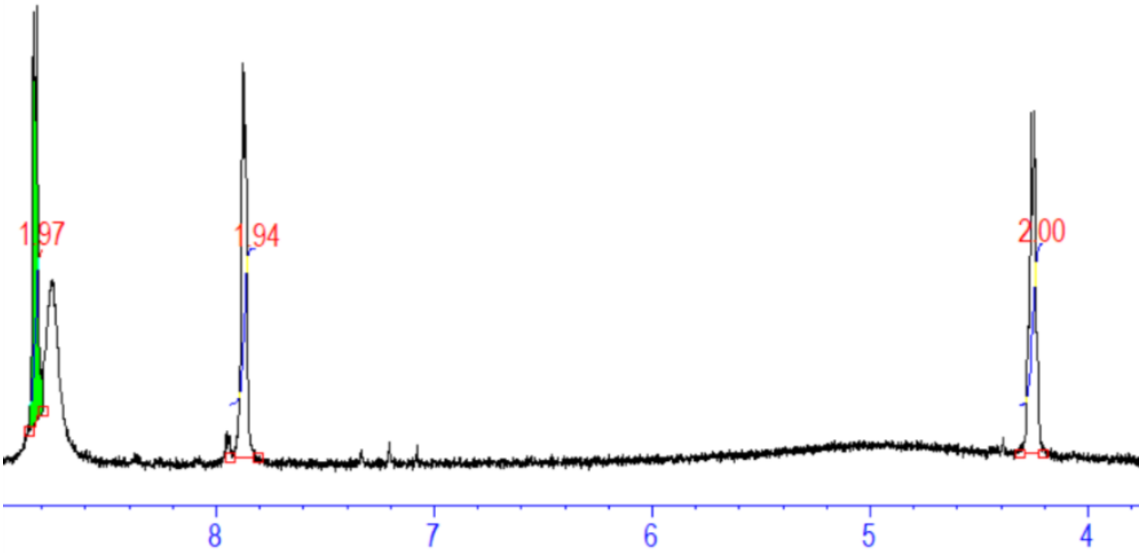

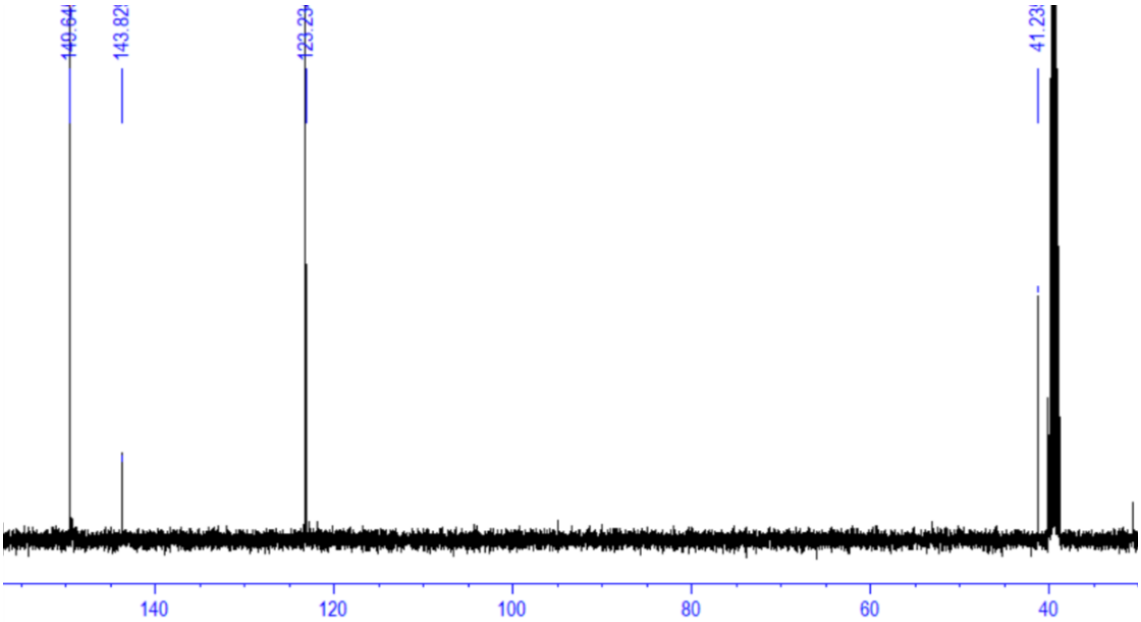

Table 1, **9b**

Furan-2-ylmethanamine hydrochloride (*S25*)

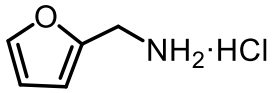

CAS registry No. [4753-68-8]. ^{1}H NMR (DMSO, 400 MHz): δ =8.50 (sbr, 3H), 7.73 (m 1H), 6.54–6.56 (m, 1H), 6.48–5.51 (m, 1H), 4.06 (m, 2H). ^{13}C NMR (DMSO, 100 MHz): 147.6, 143.8, 110.9, 110.2, 34.8.

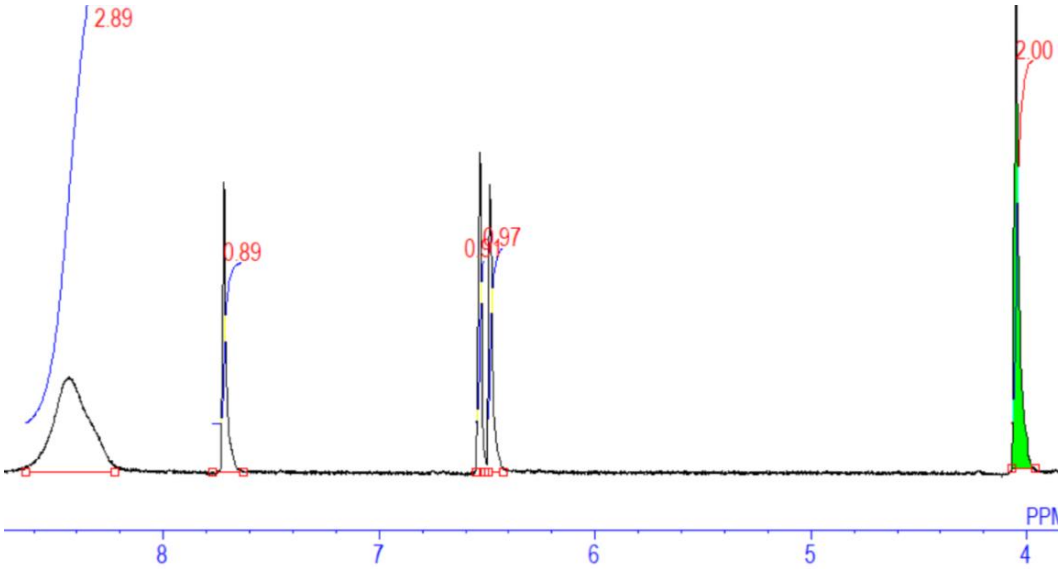

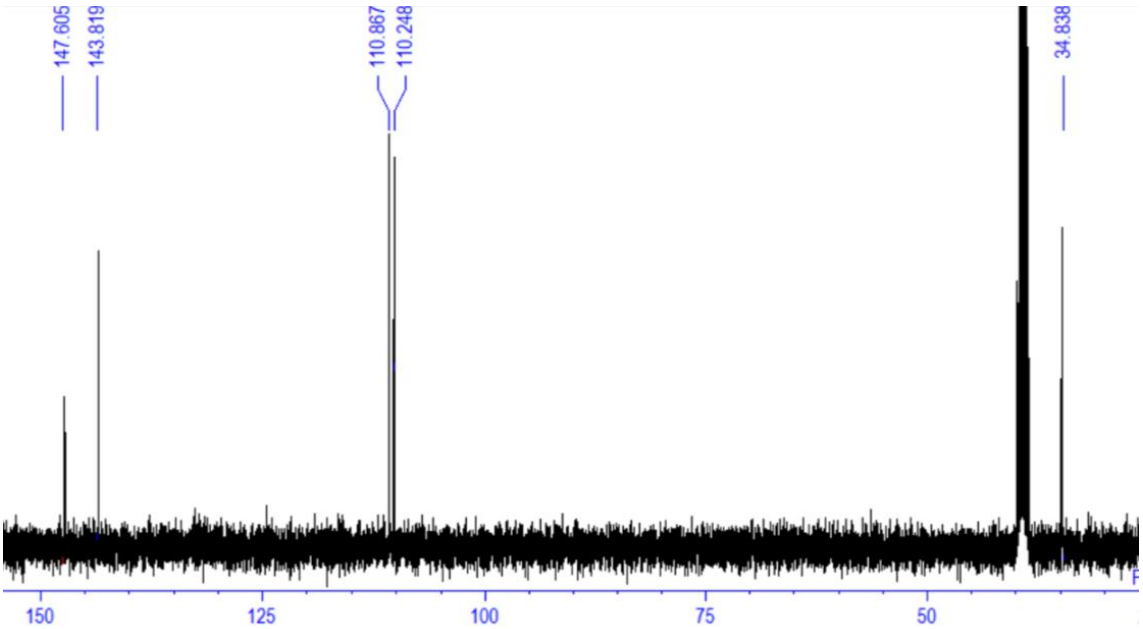

Table 1, **10b**

(1H-indol-5-yl)methanamine monohydrochloride (*S26*)

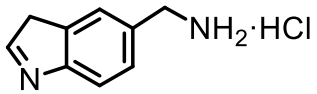

CAS registry No. [865878-77-9]. ^{1}H NMR (DMSO, 400 MHz) : δ = 10.88 (s, 1H), 8.82 (s, 3H), 7.95 (s, 1H), 7.37 (t, *J* = 2.8, 1H), 7.31 (dd, *J* = 8.4, 1.7, 1H), 7.32−7.16 (m, 2H), 4.08 (s, 2H). ^{13}C NMR (DMSO, 100 MHz): 135.6, 127.4, 126.1, 121,9, 120.8, 111.3, 100.8.

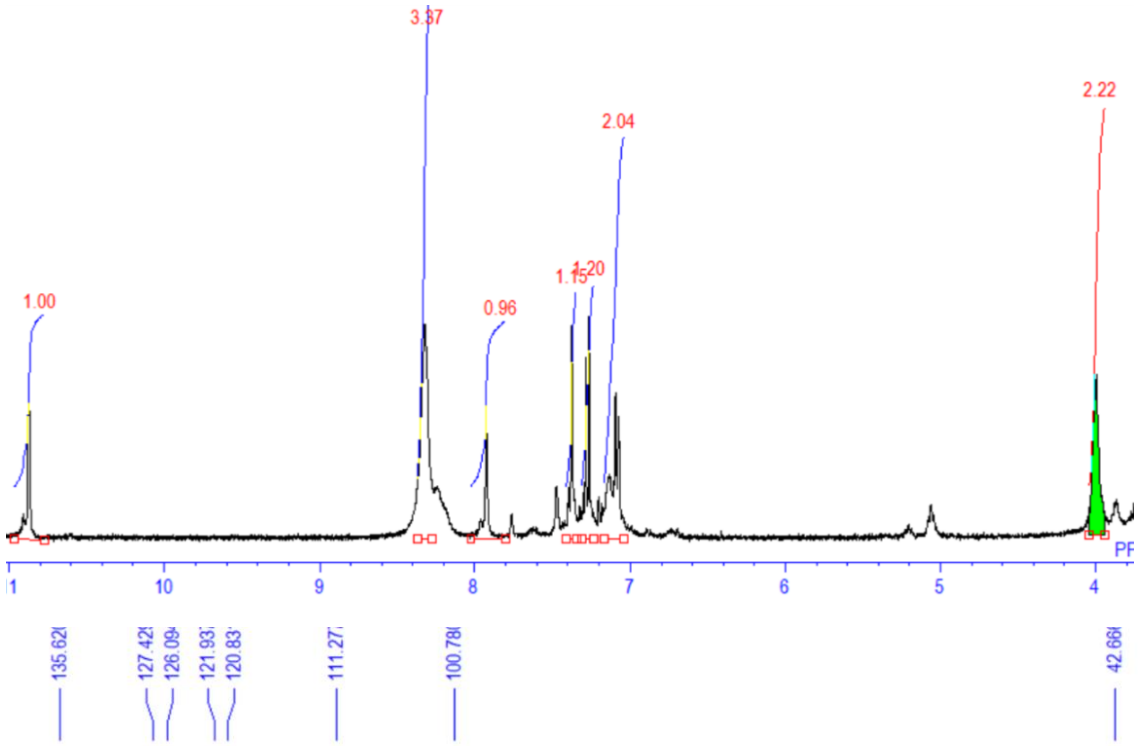

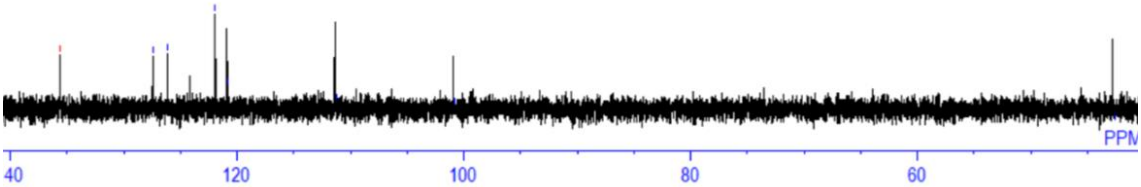

Table 1, **11b**

4-Methoxybenzylamine hydrochloride (*S21*)

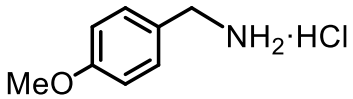

CAS registry No. [17061-61-9]. ^{1}H NMR (DMSO, 400 MHz): δ = 8.18 (s, 3H), 7.47-7.30 (m, 2H), 7.04-6.89 (m, 2H), 3.93 (s, 2H), 3.75 (s, 3H). ^{13}C NMR (DMSO, 100 MHz): 157.8, 129.4, 128.7, 113.5, 55.0, 44.0.

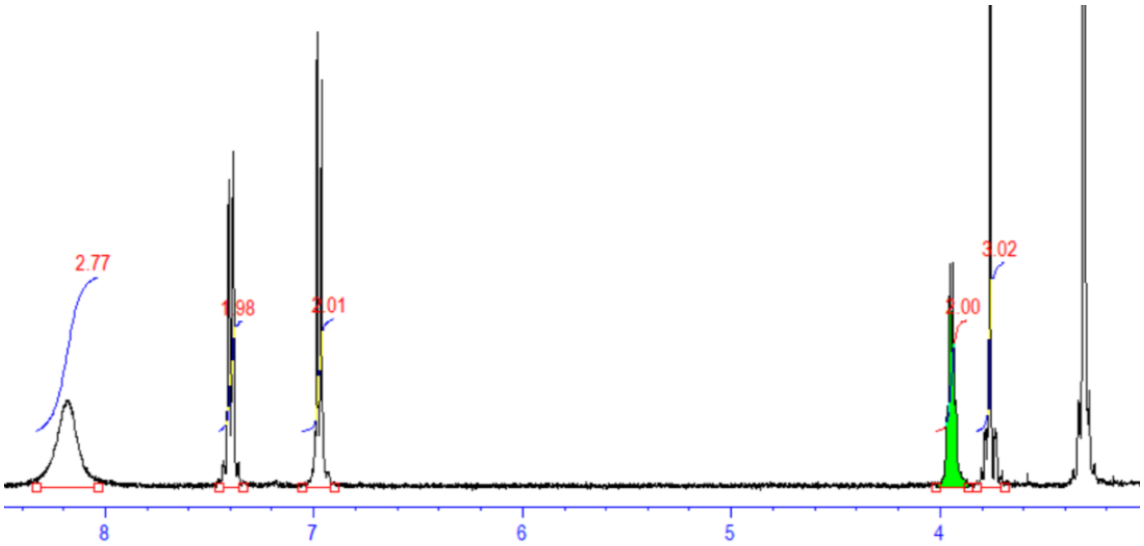

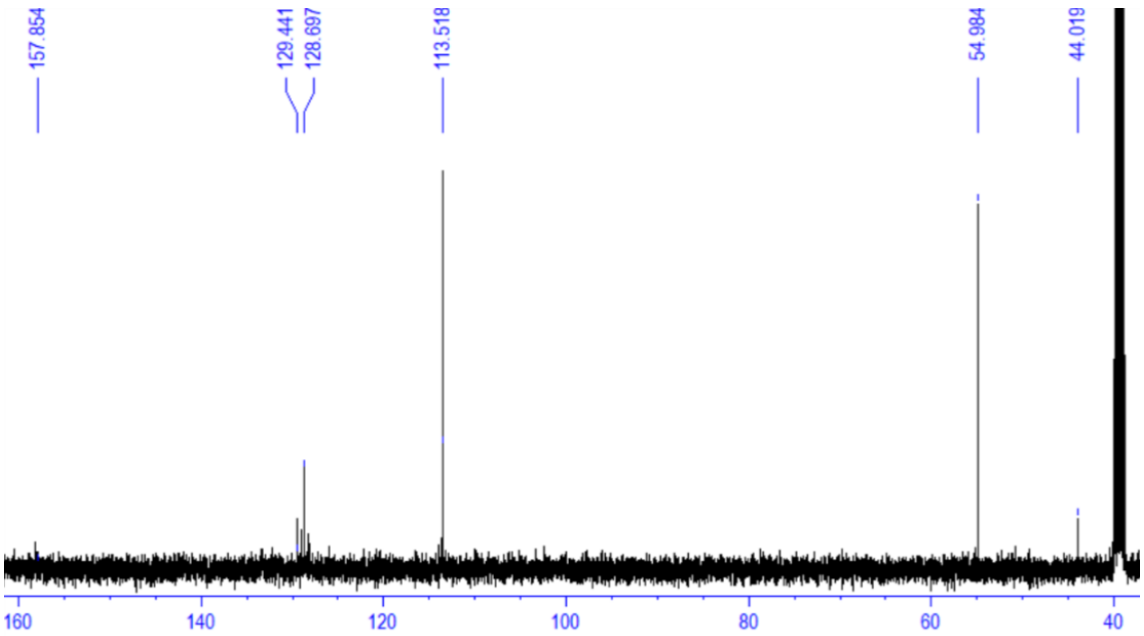

Table 1, **12b**

4-Bromobenzylamine hydrochloride (*S21*)

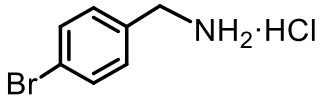

CAS registry No. [26177-44-6]. ^{1}H NMR (DMSO, 400 MHz): δ = 8.49 (s, 3H), 7.61 (d, *J* = 7.9, 2H), 7.48 (d, *J* = 7.8, 2H), 3.98 (s, 2H). ^{13}C NMR (DMSO, 100 MHz): 133.4, 131.3, 131.2, 121.6, 41.3.

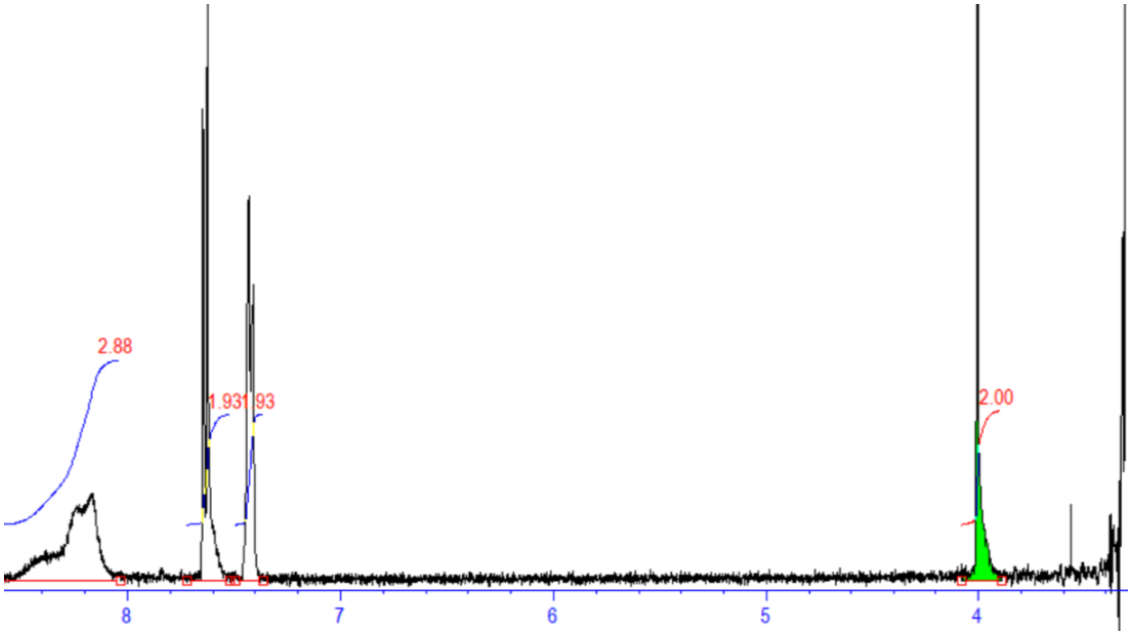

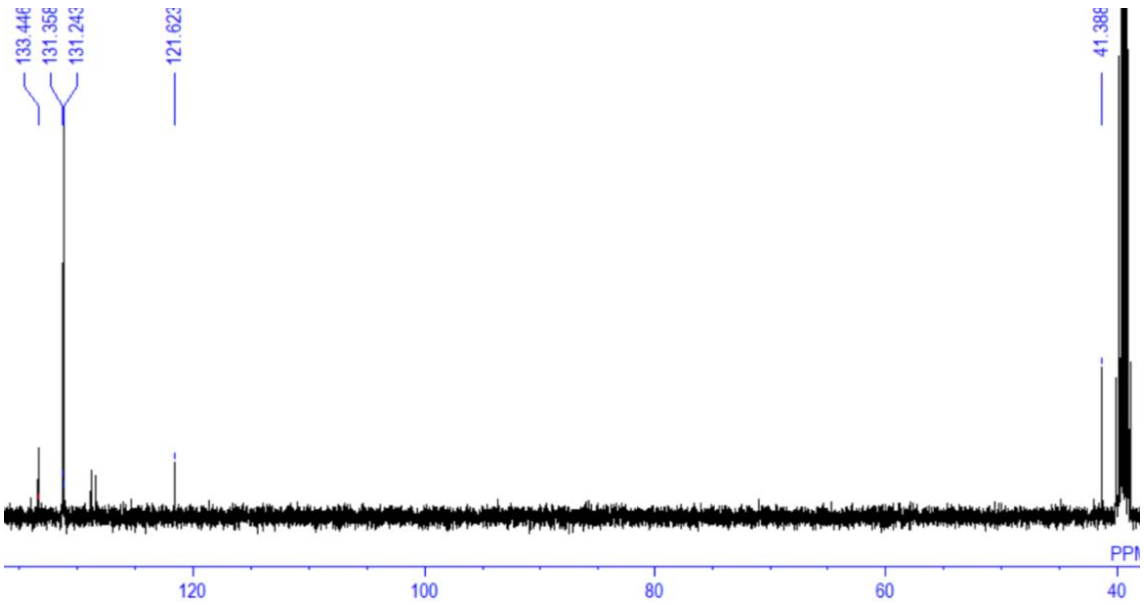

Table 1, **13b**

4-Trifluoromethylbenzylamine hydrochloride (*S21*)

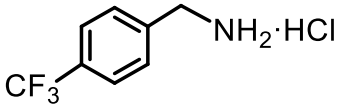

CAS registry No. [3047-99-2]. ^{1}H NMR (DMSO, 400 MHz): δ = 8.71 (s, 3H), 7.85-7.60 (m, 4H), 4.12 (s, 2H). ^{13}C NMR (DMSO, 100 MHz): 138.8, 129.7, 128.6, 125.2, 122.7, 41.5.

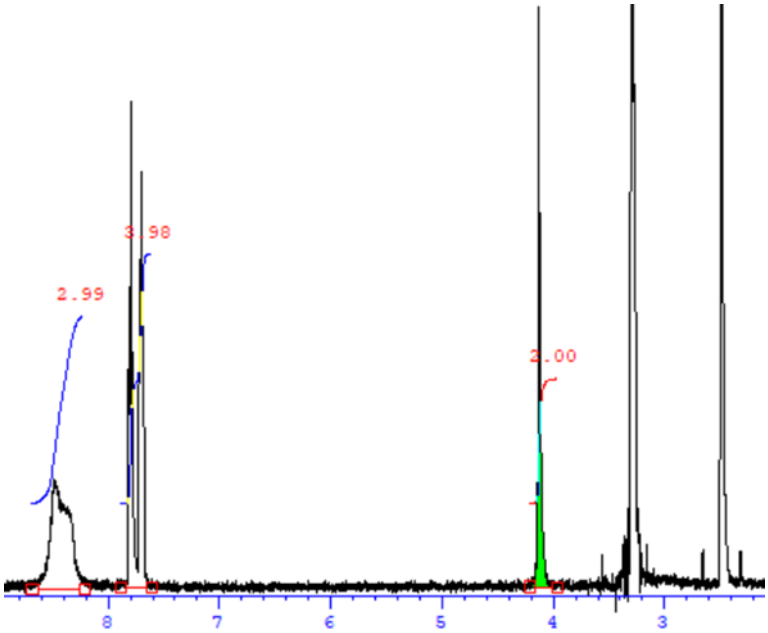

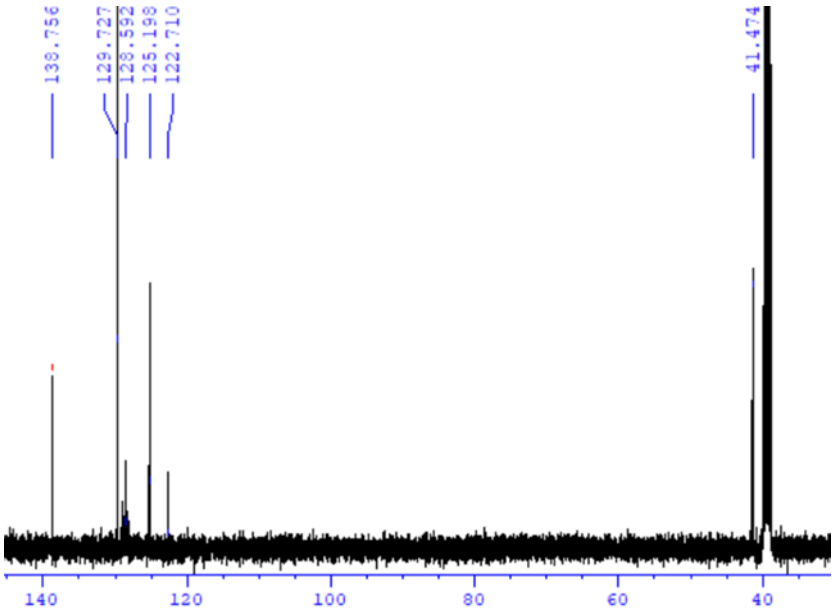

Table 1, **14b**

1-[4-(Aminomethyl)phenyl]ethan-1-one hydrochloride(*S20*)

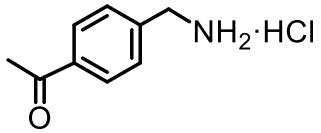

CAS registry No. [66522-66-5]. ^{1}H NMR (DMSO, 400 MHz): δ = 8.51 (s, 3H), 7.97 (d, *J* = 8.5, 2H), 7.66 (d, *J* = 8, 2H), 4.09 (s, 2H), 2.58 (s, 3H). ^{13}C NMR (DMSO, 100 MHz): 197.6, 139.1, 136.5, 129.0, 128.2, 41.6, 26.8.

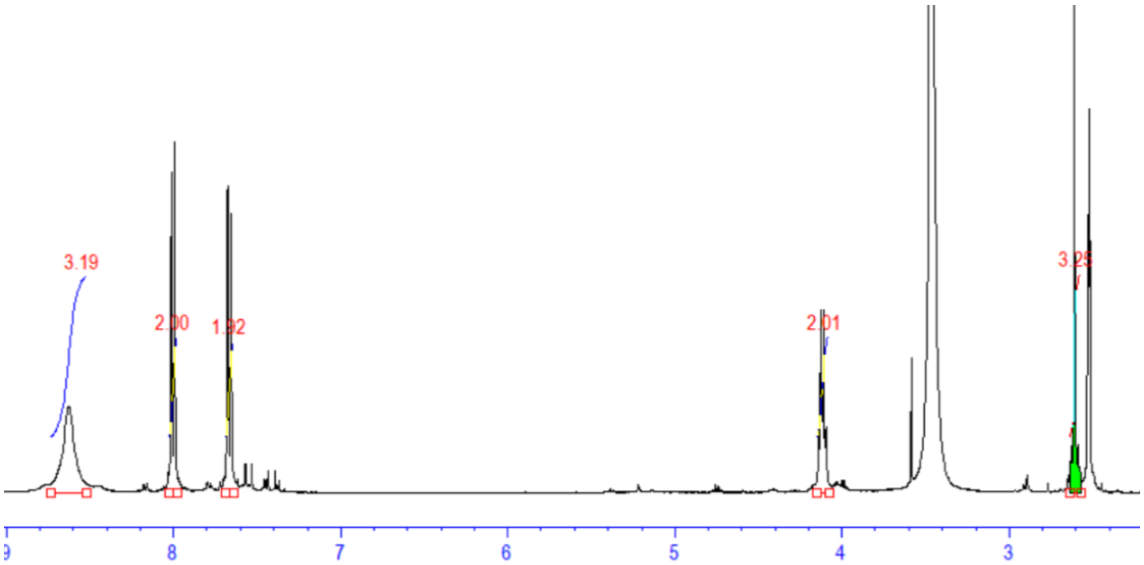

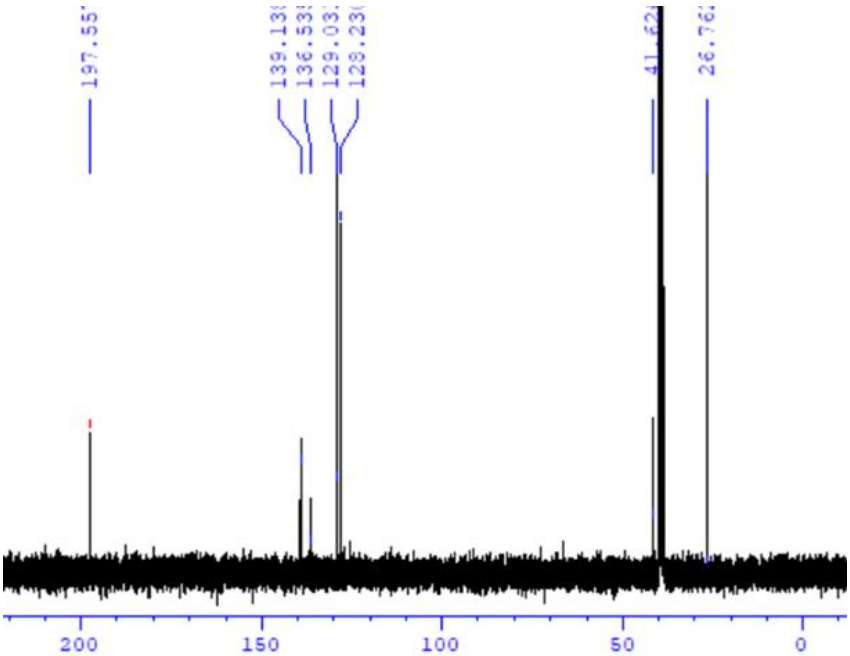

Table 1, **15b**

4-(Aminomethyl)benzoic acid methyl ester hydrochloride (*S20*)

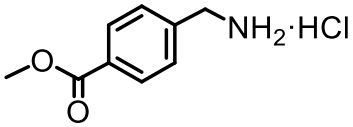

CAS registry No. [6232-11-7]. ^{1}H NMR (DMSO, 400 MHz): δ = 8.46 (s, 3H), 8.00 (d, *J* = 8.4, 2H), 7.63 (d, *J* = 8.0, 2H), 4.11 (s, 2H), 3.86 (s, 3H). ^{13}C NMR (DMSO, 100 MHz): 165.8, 129.3, 129.1, 129.0, 128.2, 52.2, 41.7.

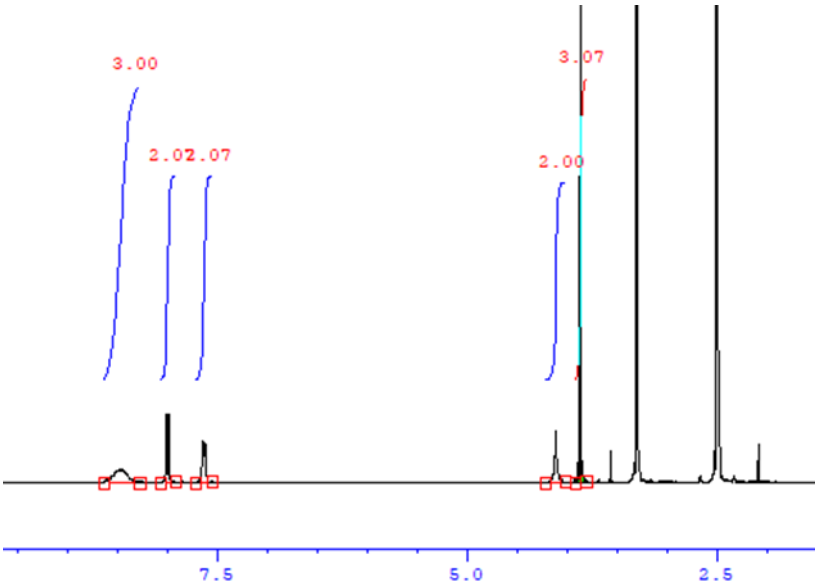

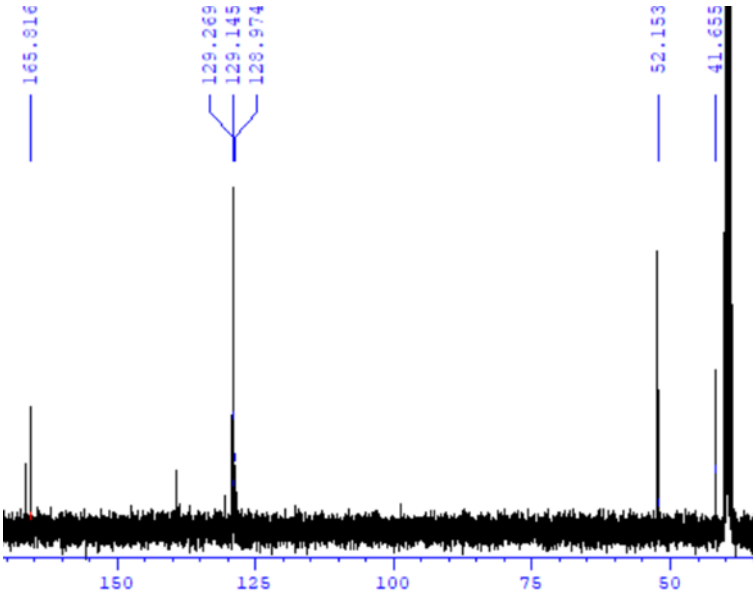

Scheme 2, **16b**

1,6-Diaminohexane dihydrochloride (*S21*)

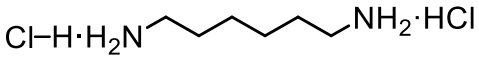

CAS registry No. [6055-52-3]. ^{1}H NMR (DMSO, 400 MHz): δ = 7.82 (s, 6H), 2.83-2.58 (m, 4H), 1.67-1.46 (m, 4H), 1.37-1.22 (m, 4H). ^{13}C NMR (DMSO, 100 MHz): 38.4, 26.6, 25.2.

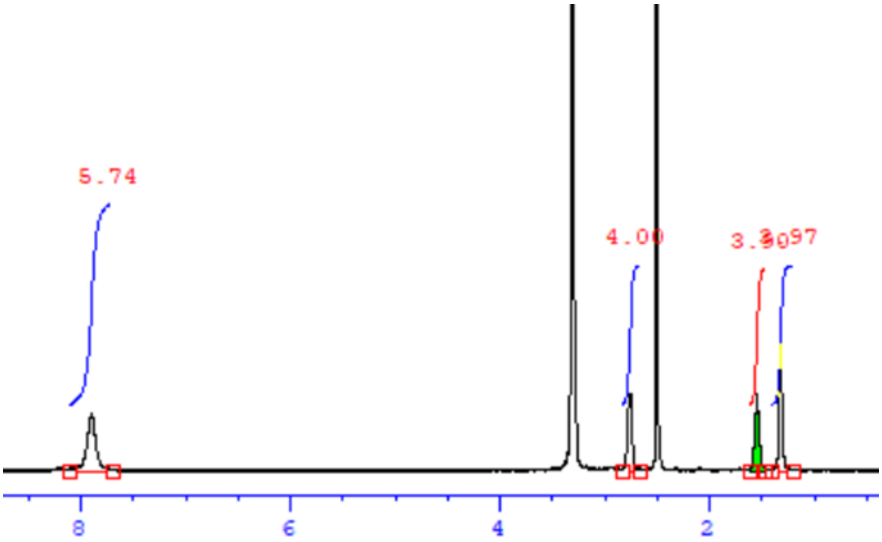

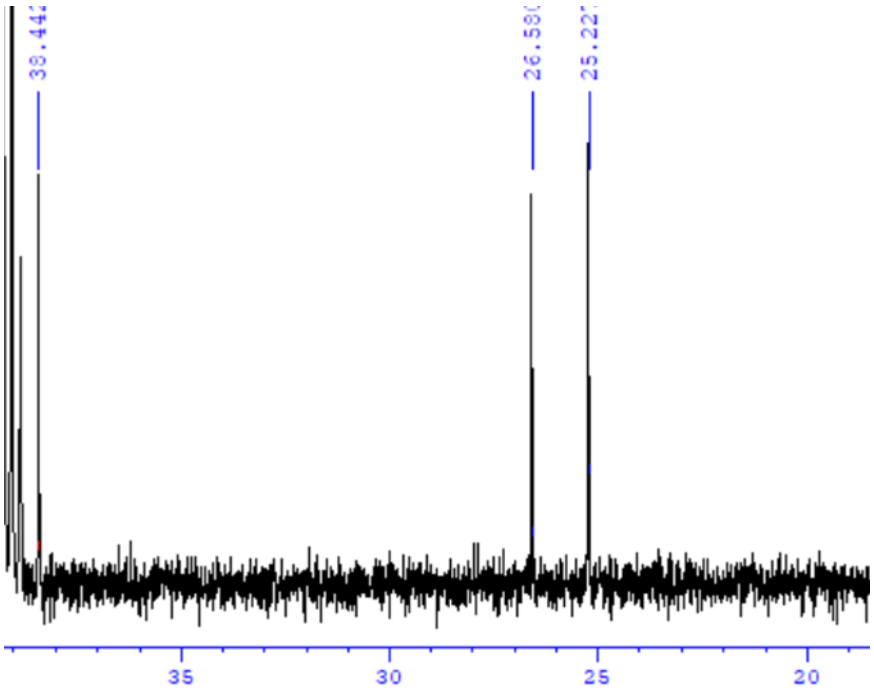

Scheme 2, 17b

1,10-diaminodecane dihydrochloride (*S20*)

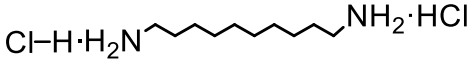

CAS registry No. [7408-92-6]. ^{1}H NMR (DMSO, 400 MHz): δ = 8.08 (s, 6H), 2.71 (m, 4H), 1.55 (m, 4H), 1.26 (m, 12H). ^{13}C NMR (DMSO, 100 MHz): 38.6, 28.6, 28.4, 26.8, 25.7.

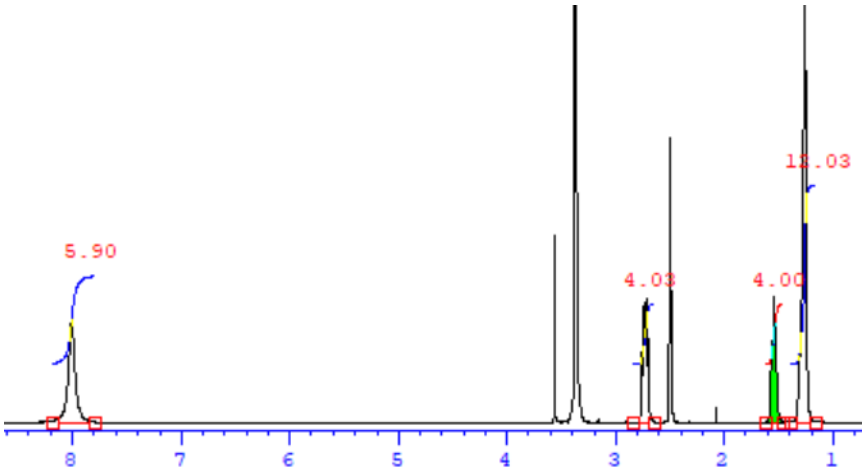

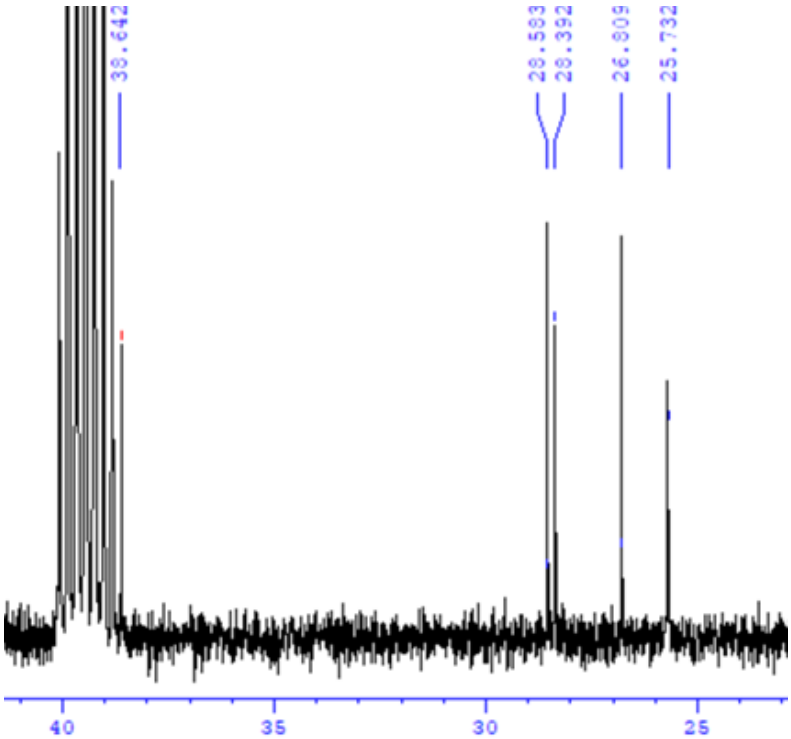

Scheme 2, **18b**

1,4-Bis(aminomethyl)benzene dihydrochloride (*S28*)

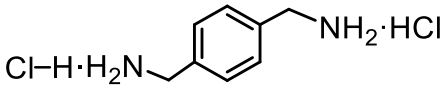

CAS registry No. [3057-45-2]. ^{1}H NMR (DMSO, 400 MHz): δ = 8.48 (s, 6H), 7.50 (s, 4H), 4.01 (s, *4*H). ^{13}C NMR (DMSO, 100 MHz): 134.2, 128.6, 41.8.

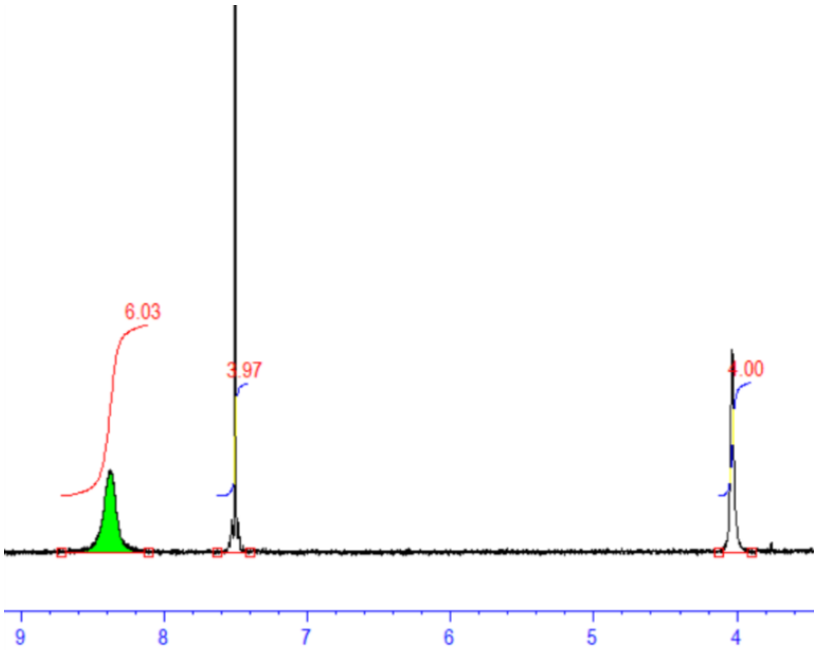

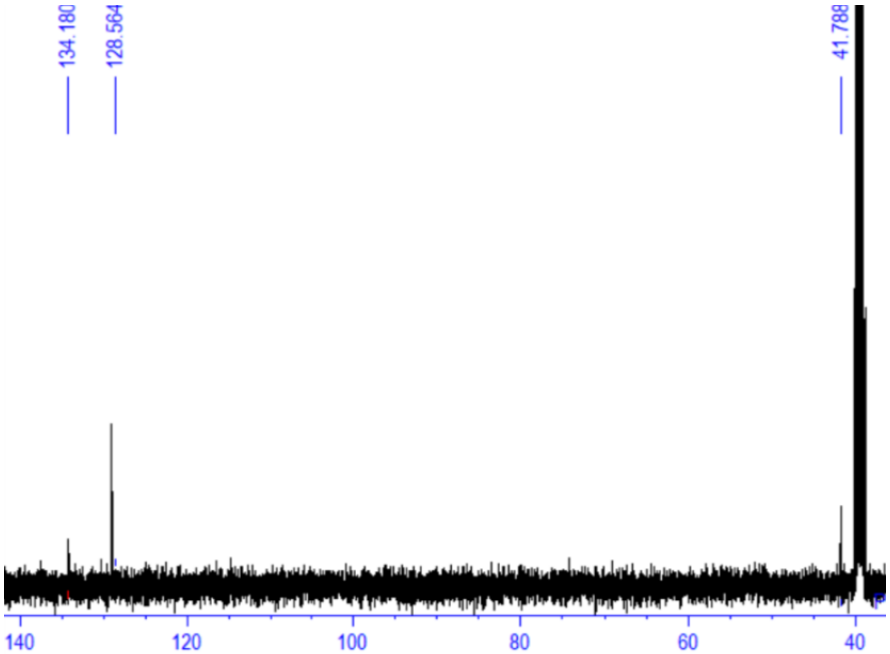

Scheme 2, **19b**

***m*-Xylylenediamine dihydrochloride (*S28*)**

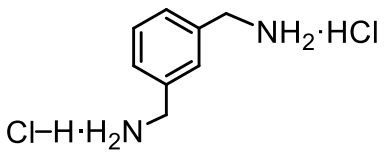

CAS registry No. [51964-30-8]. ^{1}H NMR (DMSO, 400 MHz): δ = 8.66 (s, 6H), 7.61 (d, J = 1.9 Hz, 1H), 7.55 (dd, J = 7.4, 1.8 Hz, 2H), 7.45 (dd, J = 8.4, 6.9 Hz, 1H), 3.99 (s, 4H). ^{13}C NMR (DMSO, 100 MHz): 134.3, 129.6, 128.8, 128.6, 41.9.

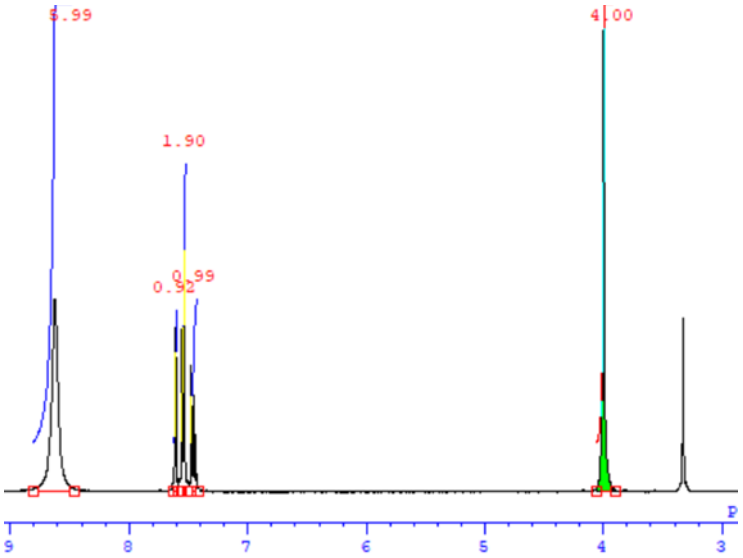

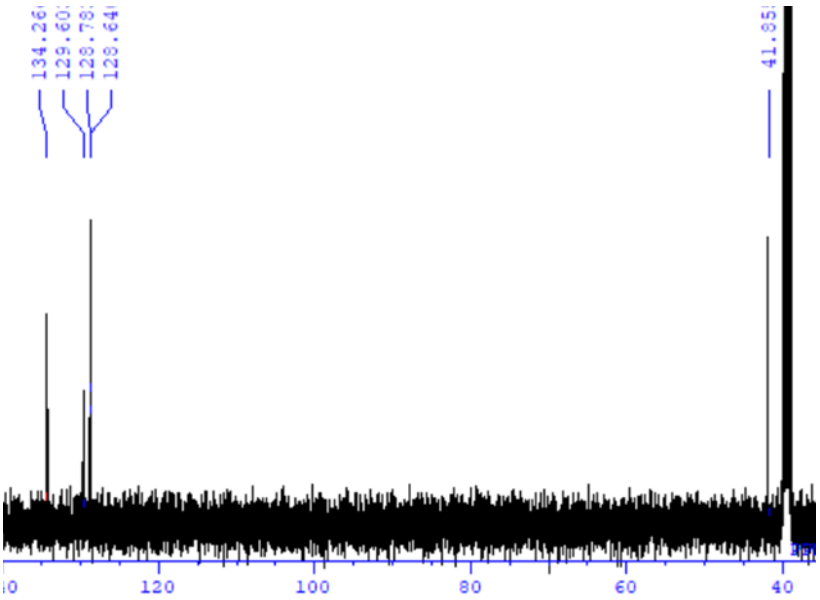

Scheme 2, **20b**

***N,N,N',N'*-Tetrakis(3-aminopropyl)-1,4-butanediamine (*S27*)**

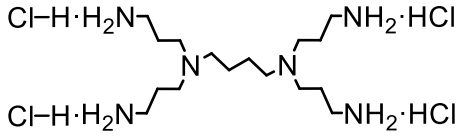

CAS registry No. [120239-63-6]. 1H NMR ($CDCl_3$, 400 MHz): δ = 2.83 (t, 8H), 2.62 (t, 8H), 2.41 (m, 4H), 1.78(t, 8H), 1.60(m, 4H), 1.48(m, 8H). ^{13}C NMR ($CDCl_3$, 100 MHz): 53.6, 51.4, 40.3, 31.4, 24. 5.

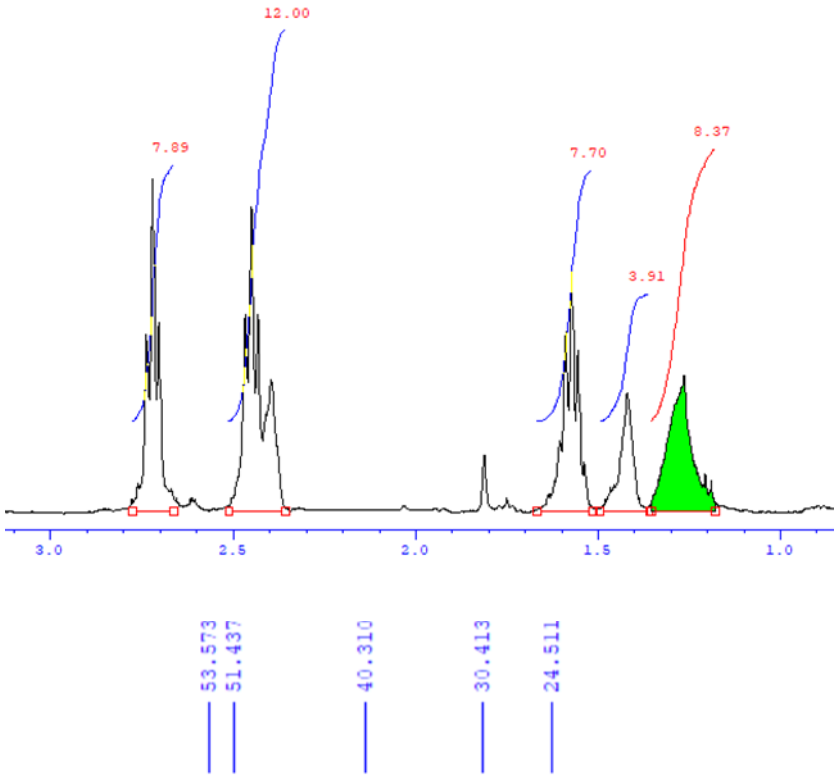

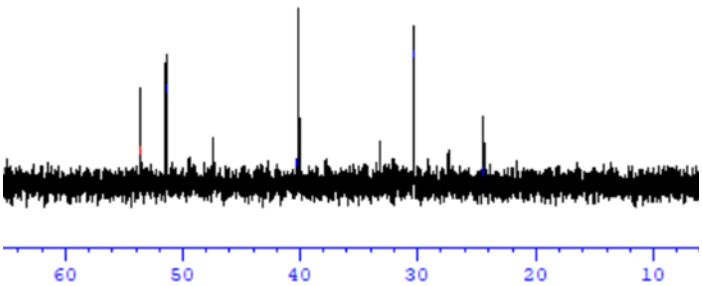

References

S1. R. Beltrán-Suito, P. Menezes and M. Driess, *J. Mater. Chem. A*, 2019, **7**, 15749-15756.

S2. R. Zhang, P. Russo, M. Feist, P. Amsalem, N. Koch and N. Pinna, *ACS Appl. Mater. Interfaces* 2017, **9**, 14013−14022.

S3. M. Liu, L. Yang, T. Liu, Y. Tang, Sa. Luo, C. Liu and Y. Zeng, *J. Mater. Chem. A*, 2017, **5**, 8608.

S4. Y. Chen, Z. Chen, Y. Lin and Y. Hsu, *ACS Sustainable Chem. Eng*. 2017, **5**, 3863−3870.

S5. D. Ha, L. Moreau, C. Bealing, H. Zhang, R. Hennig and R. Robinson, *J. Mater. Chem.*, 2011, **21**, 11498-11510.

S6. M. Elizabeth Mundy, D. Ung, N. Lai, E. Jahrman, G. Seidler and B. Cossairt, *Chem. Mater.* 2018, **30**, 5373-5379.

S7. D. Li, H. Baydoun, B. Kulikowski and S. Brock, *Chem. Mater*. 2017, **29**, 3048−3054.

S8. S. Liu, X. He, J. Zhu, L. Xu and J. Tong, *Sci. Rep.*, 2016, **6**, 35189.

S9. H. Li, F. Ke and J. Zhu, *Nanomaterials*, 2018, **8**, 89.

S10. J. Wang, L. Zhu, G. Dharan and G. Ho, *J. Mater. Chem. A*, 2017,**5**, 16580-16584.

S11. Conquest website, http://www.order-n.org, (accessed March 2019), the code is available as part of a beta test and will be freely released soon.

S12. J. P. Perdew, K. Burke and M. Ernzerhof, *Phys. Rev. Lett.* 1996, **77**, 3865–3868.

S13. A. S. Torralba, *J. Phys.: Condens. Matter*, 2008, **20**, 294206.

S14. H. J. Monkhorst and J. D. Pack, *Phys. Rev. B* 1976, **13**, 5188–5192.

S15. The Photographic Periodic Table of the Elements Home Page, http://periodictable.com (accessed March 2019).

S16. S. Rundqvist, *Anorg. Allg. Chem*. 2001, **627**, 2257–2260.

S17. Z. Yang, L. Liu, X. Wang, S. Yang and X. Su, *J. Alloys Compd*. 2011, **509**, 165–168.

S18. S. Grimme, *J. Comp. Chem.* 2006, **27**, 1787–1799.

S19. F. B. van Duijneveldt, J. G. C. M. van Duijneveldt-van de Rijdt and J. H. van Lenthe, *Chem. Rev*. 1994, **94**, 1873–1885.

S20. K. Tokmic, B. Jackson, A. Salazar, T. Woods and A. Fout, *J. Am. Chem. Soc.* 2017, **139**, 13554–13561.

S21. F. Chen, C. Topf, J. Radnik, C. Kreyenschulte, H. Lund, M. Schneider, A. Surkus, L. He, K. Junge and M. Beller, *J. Am. Chem. Soc.* 2016, **138**, 8781–8788.

S22. S. Elangovan, C. Topf, S. Fischer, H. Jiao, A. Spannenberg, W. Baumann, R. Ludwig, K. Junge and M. Beller, *J. Am. Chem. Soc*. 2016, **138**, 8809–8814.

S23. B. Paul, K. Chakrabatri and S. Kundu, *Dalton Trans.* 2016, **45**, 11162–11171.

S24. Z. Lu and T. Williams, *Chem. Commun.* 2013, **50**, 5391–5393.

S25. S. Wübbolt and M. Oestreich. *Synlett* 2017, **18**, 2411–2414.

S26. N. Gandhamsetty, J. Jeong, J. Park, S. Park and S. Chang, *J. Org. Chem.* 2015, **80**, 7281–7287.

S27. M. Daniel, J. Ruiz and D. Astruc, *J. Am. Chem. Soc.* 2003, **125**, 1150–1151.

S28. M. Heilmann and K. Tiefenbacher, *Chem. Eur.J.* 2019, **25**, 12900–12904.